

PREDICTIONS OF WAVE HEIGHTS IN
THE LAGOON OF FLIC-EN-FLAC,
UNDER SEA LEVEL RISE
PROJECTIONS FOR THE MEAN AND
EXTREME WAVE CLIMATES USING
THE SWAN SPECTRAL MODEL

TREBALL FINAL DE MÀSTER

Thesis completed by:
Claude la Hause de Lalouviere

Under the supervision of:
Vicenc Gracia Garcia
Juan Pablo Sierra Pedrico
Manuel Garcia-Leon

Master in:
**Coastal and Marine Engineering
and Management (CoMEM)**

Barcelona, 15 June 2018

Departament d'Enginyeria Civil i Ambiental

ERASMUS +: ERASMUS MUNDUS MOBILITY PROGRAMME

Master of Science in

COASTAL AND MARINE ENGINEERING AND
MANAGEMENT

CoMEM

**PREDICTIONS OF WAVE HEIGHTS IN THE LAGOON OF FLIC-EN-FLAC, UNDER
SEA LEVEL RISE PROJECTIONS FOR THE MEAN AND EXTREME WAVE
CLIMATES USING THE SWAN SPECTRAL MODEL**

Polytechnic University of Catalonia
15 June 2018

Claude la Hausse de Lalouviere

The Erasmus+: Erasmus Mundus MSc in Coastal and Marine Engineering and Management is an integrated programme including mobility organized by five European partner institutions, coordinated by Norwegian University of Science and Technology (NTNU).

The joint study programme of 120 ECTS credits (two years full-time) has been obtained at two or three of the five CoMEM partner institutions:

- Norges Teknisk- Naturvitenskapelige Universitet (NTNU) Trondheim, Norway
- Technische Universiteit (TU) Delft, The Netherlands
- Universitat Politècnica de Catalunya (UPC). BarcelonaTech. Barcelona, Spain
- University of Southampton, Southampton, Great Britain
- City University London, London, Great Britain

During the first three semesters of the programme, students study at two or three different universities depending on their track of study. In the fourth and final semester an MSc project and thesis has to be completed. The two-year CoMEM programme leads to a multiple set of officially recognized MSc diploma certificates. These will be issued by the universities that have been attended by the student. The transcripts issued with the MSc Diploma Certificate of each university include grades/marks and credits for each subject.

Information regarding the CoMEM programme can be obtained from the programme coordinator:

Øivind A. Arntsen, Dr.ing.
Associate professor in Marine Civil Engineering
Department of Civil and Environmental Engineering
NTNU Norway
Mob.: +4792650455 Fax: + 4773597021
Email: oivind.arntsen@ntnu.no

CoMEM URL: <https://www.ntnu.edu/studies/mscomem>

Disclaimer:

"The European Commission support for the production of this publication does not constitute an endorsement of the contents which reflects the views only of the authors, and the Commission cannot be held responsible for any use which may be made of the information contained therein."

CoMEM Thesis

This thesis was completed by:

Claude la Hause de Lalouviere

Under supervision of:

Vicente Gracia Garcia, Associate Professor at the Polytechnic University of Catalonia (EHMA)

Joan Pablo Sierra Pedrico, Professor at the Polytechnic University of Catalonia (EHMA)

Manuel García-León, Researcher, Marine Engineering Laboratory (LIM/UPC)

As a requirement to attend the degree of

*Erasmus+: Erasmus Mundus Master in Coastal and Marine Engineering and Management
(CoMEM)*

Taught at the following educational institutions: [delete those not proper]

Norges Teknisk- Naturvitenskapelige Universitet (NTNU)

Trondheim, Norway

Universitat Politècnica de Catalunya, (UPC). BarcelonaTech.

Barcelona, Spain

University of Southampton,

Southampton, Great Britain

At which the student has studied from August 2016 to July 2018.

Abstract

Barrier reefs regulate the morphodynamics of its inbounded shorelines, in dissipating most of the incoming wind generated waves. Climate change effects, such as sea level rise and reef degradation may compromise the capacity of reefs to continue providing their coastal protective services. The significant wave height inside the barrier reef protected lagoon of Flic-en-flac is determined with the SWAN (Simulating WAves Nearshore) wave model for futuristic scenarios of increased sea levels and degraded coral reefs. Both the mean wave climate and single extreme event conditions are considered. The results indicate that a lower coral structure complexity induces higher waves protruding over the reef. Likewise, for higher water levels, higher wave heights reach the lagoon, as a consequence of less depth induced breaking occurring. Overall, when modelling outputs from the projected reef and sea water level conditions in 2100 are compared with the reference condition results, increases of high magnitude in wave heights are observed. The findings indicate that if the reef evolves under the proposed pessimistic scenarios, major hydrodynamic changes will occur, threatening the condition of the shoreline. Similarly, under cyclonic conditions, which periodically causes major coastal alterations; the repercussions of increases in the wave height reaching the shore could see an increase in the magnitude and frequency of such beach morphodynamic changes.

Acknowledgements

Firstly, I would like to thank my professors and mentors: Vicenç, Joan Pau and Manuel for their guidance, recommendations and patience. I really appreciate the enthusiasm you have shared for my research topic which relates to my home country. Working with you has allowed me to develop an even stronger appreciation of the Mediterranean warmth, humor and kindness.

Secondly, I would like to thank the organizations, institutions and companies who have shared some valuable information to help with my work. All the staff at the MOI for corresponding and sharing wave data and bathymetric maps relating to the study site. The MMCS for sharing valuable information about the study area. And Baird & Associates for sharing some of their report appendices.

Thirdly, I would like to thank my family and friends who have been very supportive throughout these past months. Particularly my sister for her valuable suggestions. I cannot forget my day to day companion Johno, with who I've spent many hours studying, discussing concepts, debating thesis unrelated topics, sharing opinions and extremely spicy foods.

Finally, I would like to thank: the European Commission for the support to the CoMEM program. The program coordinators: Oivind and Sonja for their continual help with any logistical inquiry; while always being examples of humility and gentleness. My professors at the three Universities (UPC, SOTON, NTNU) I have attended over the last two years. Likewise, I would like to extend my gratitude to Cesar, the UPC program coordinator who greeted us in Barcelona with incredible care.

This thesis was prepared during the 4th semester of the CoMEM program, in Spain. It comes after culturally diverse learning experiences from previous terms in Norway, Spain and the UK. Partaking in this wonderful journey, I have had the opportunity to discover beautiful places, and people; in rich multi-cultural settings. I feel extremely privileged to have shared these experiences, over part of these last two years, with every single person in my cohort.

C. la Hausse de Lalouviere
Barcelona, June 2018

Contents

LIST OF FIGURES.....	XIV
NOMENCLATURE.....	XV
INTRODUCTION.....	1
<i>Problem definition.....</i>	2
<i>Research Approach</i>	2
LITERATURE REVIEW.....	3
2.1 CLIMATE PREDICTIONS GIVEN IN THE AR5 OF THE IPCC.....	3
2.1.1 <i>Introduction.....</i>	3
2.1.2. <i>Sea level rise.....</i>	4
2.1.3. <i>Ocean Temperature.....</i>	5
2.1.4. <i>Ocean Acidity.....</i>	5
2.1.5. <i>Global reef survival predictions.....</i>	5
2.1.6. <i>Wave climate variations.....</i>	6
2.1.7. <i>Cyclonic events variations.....</i>	7
DESCRIPTION OF STUDY AREA.....	8
3.1 GENERAL DESCRIPTION.....	8
3.2 MORPHOLOGY.....	9
3.2.1 <i>General geology.....</i>	9
3.2.2 <i>Coastal geology</i>	9
3.3 REEF AS A SEDIMENT SOURCE	10
3.3.1 <i>Sediment source.....</i>	10
3.3.2 <i>Energy dissipater.....</i>	10
3.4 WAVE CLIMATE OF MAURITIUS	10
3.4.1 <i>Climatic systems, winds and resulting waves</i>	10
3.4.2 <i>Wave climate data available.....</i>	12
3.5 TIDAL REGIME	13
3.6 SEA LEVEL RISE	14
3.6.1 <i>Global Historical sea level rise</i>	14
3.6.2 <i>Recent Sea level rise trends in Mauritius.....</i>	15
3.7 CURRENT STATE OF THE FLIC-EN-FLAC CORAL BARRIER AND FRINGING REEF.....	15
3.8 PROJECTIONS OF THE FUTURE STATE OF THE REEF IN FLIC-EN-FLAC (1986-2100).....	16
METHODOLOGY	17
4. 1 MODEL SET-UP – MEAN WAVE CLIMATE.....	17
4.1.1 <i>Procedure</i>	17

4.1.2 Scenarios – mean wave conditions.....	18
4.1.4 Wave input.....	20
4.1.4.1 Wave input – Scenario 7.....	21
4.1.5 Model domains	22
4.1.6 Bathymetry.....	23
4.1.7 Tide input	24
4.1.8 Friction.....	24
4.1.9 SWAN parameters.....	25
4.2 MODEL SET-UP - EXTREME WAVE CLIMATE	26
4.2.1 Procedure	26
4.2.2 Scenarios – Extreme wave climate	26
4.2.5 Model domains	30
4.2.6 Tide	30
4.2.7 Surge	31
NUMERICAL MODEL RESULTS	32
5.1 MEAN WAVE CLIMATE	32
5.1.1 Qualitative calibration.....	33
5.1.2 Tidal effects on energy dissipated.....	33
5.1.3 SLR effects on SWH.....	36
5.1.4 Friction coefficient.....	38
5.1.5 Energy levels.....	40
5.1.6 Effect of wave setup	41
5.1.7 Effect of increased wave climate	42
5.2 EXTREME WAVE CLIMATE.....	43
LIMITATIONS	48
6.1 DATA AVAILABILITY	48
6.1.1 Wave data	48
6.1.2 Bathymetry.....	49
6.2 MODELLING LIMITATIONS	49
6.3 ANALYSIS.....	50
DISCUSSION AND CONCLUSION.....	51
REFERENCES.....	54

List of figures

FIGURE 1: CO ₂ EMISSIONS FOR THE REPRESENTATIVE CONCENTRATION PATHWAYS (IPCC, 2014)	3
FIGURE 2: PROJECTIONS FROM PROCESS-BASED MODELS OF (A) GLOBAL MEAN SEA LEVEL (GMSL) RISE RELATIVE TO 1986–2005 FOR RCP4.5 AND RCP8.5 (CHURCH ET AL., 2013).....	4
FIGURE 3: MEAN REGIONAL SEA LEVEL CHANGE (M) EVALUATED FROM 21 CMIP5 MODELS FOR RCP4.5 (LEFT) AND RCP8.5 (RIGHT) (CHURCH ET AL., 2013).....	4
FIGURE 4: A) PERCENT CHANGE SWH BETWEEN THE PERIODS OF 2075-2100 AND 1980 -2009, B) FOR MONTHS OF JANUARY TO MARCH, C) FOR MONTHS OF JULY TO SEPTEMBER (CHURCH ET AL., 2013)	6
FIGURE 5: MAP OF THE STUDY AREA -FLIC EN FLAC LAGOON (GOOGLE EARTH, ACCESSED ON MAY25, 2018)	8
FIGURE 6: TYPICAL CROSS SECTION OF A TROPICAL REEF (NOAA, 2017)	9
FIGURE 7: GLOBAL PRESSURE SYSTEMS DURING THE AUSTRAL SUMMER (NCAR, 2011).....	11
FIGURE 8: GLOBAL PRESSURE SYSTEMS DURING THE AUSTRAL WINTER (NCAR, 2011).....	11
FIGURE 9: TIDAL VARIATIONS OVER MAY AND JUNE 2018, IN MAURITIUS (ACD)	13
FIGURE 10: SEA LEVEL CHANGE FROM THE LAST GLACIAL PERIOD BASED ON SITES IN DIFFERENT GLOBAL LOCATIONS (FLEMING ET AL., 1998).....	14
FIGURE 11: <i>SEA LEVEL RISE AT DIFFERENT WORLDWIDE SITES AND FROM TIDE GAUGE RECONSTRUCTIONS</i> (CHURCH ET AL., 2013).....	14
FIGURE 12: TREND OF AVERAGE SEA LEVELS IN MAURITIUS (1987-2017).....	15
FIGURE 13: FLOWCHART OF THE PROCEDURE FOLLOWED FOR EACH MEAN WAVE CLIMATE SCENARIO	17
FIGURE 14: WAVE ROSE BASED ON 39 YEARS OF ERAINTERIM DATA.....	19
FIGURE 15: INTERVAL OF MEAN WAVE DIRECTIONS CONSIDERED FOR THE SWAN RUNS.....	20
FIGURE 16: GRAPH SHOWING THE RELATIONSHIP BETWEEN THE MEAN PERIOD AND WAVE HEIGHT.....	21
FIGURE 17: COMPUTATIONAL BOUNDARIES OF SWAN DOMAINS	22
FIGURE 18: REEF CROSS-SECTION REPRESENTING THE TYPICAL BATHYMETRIC DIMENSIONS.....	23
FIGURE 19: FLOWCHART OF THE PROCEDURE FOLLOWED FOR EACH EVENT	26
FIGURE 20: WAVE ROSE FROM ERAINTERIM DATA [57° E AND 20.25°S] USED FOR THE EXTREME CLIMATE	27
FIGURE 21: DOMAINS OF THE RUNS FOR THE EXTREME CLIMATE.....	30
FIGURE 22: EVOLUTION OF THE SWH ACROSS SECTION 2 FOR ALL SCENARIOS.....	32
FIGURE 23: WAVE DECAY AT CROSS SECTION 2 – UPPER LIMIT REPRESENTED WITH THE HIGHEST ASTRONOMICAL TIDE (Sc5)33	33
FIGURE 24: SWH AT SCENARIOS 1-3 & 5 ALONG SECTION 2.....	36
FIGURE 25: SWH VS SLR SCENARIOS – FROM THE SWH AT A POINT GIVEN Sc1-3, 5, 6 RESULTS.....	37
FIGURE 26: DIFFERENCE IN THE SWH BETWEEN THE REFERENCE AND Sc4 ACROSS SECTION 2 OF THE REEF	39
FIGURE 27: WAVE ENERGY PER SURFACE AREA FOR REF, Sc1 AND Sc2.....	40
FIGURE 28: COMPARISON OF SETUP EFFECTS IN THE REFERENCE SCENARIO AND SCENARIO 1	41
FIGURE 29: SWH CROSS SECTION FOR Sc1 AND Sc3 FROM THE FORE REEF TO SHORE.	42
FIGURE 30: PLOT OF SWH EVOLUTION OVER REEF FOR WAVE CONDITIONS OF DIFFERENT RETURN PERIODS FOR THE PRESENT CONDITIONS	43

Nomenclature

Abbreviations	Description
ACD	Admiralty Chart Datum
AR 5	Fifth Assessment Report
ECMWF	European Centre for Medium-Range Forecasts
GHG	Greenhouse Gas
HAT	Highest Astronomical Tide
IPCC	International Panel for Climate Change
LAT	Latitudinal
LMSL	Local Mean Sea Level
LONG	Longitudinal
MSWH	Mean Significant Wave Height
MWS	Mean Wind Speed
POT	Peak Over Threshold
RCP	Representative Concentration Pathway
RP	Return Period
Sc	Scenario
SLR	Sea Level Rise
SWAN	Simulating WAve Nearshore
SWH	Significant Wave Height (m)

1

Introduction

The beaches in Mauritius have a high socio economic importance for the country. On the west coast of the island, the beach of Flic-en-flac has seen an increase in both the local and tourist recreational users over the last decades. Given this is a limited resource; the increase in the number of users results in the high importance to maintain and preserve it. In recent years, Flic-en-flac has experienced recurring erosion events and has been classified as a beach of high management priority in terms of erosion risks, in past assessment reports (JICA, 2015), (Baird, 2003).

The dynamics of the shoreline in Flic-en-flac are governed by the wave conditions which traverse the reef and reach the shore. The coral reef bordering the lagoon provides a protection barrier for dissipating wave energy away from the shoreline. It regulates the sediment budget, and protects the shoreline and near shore infrastructure from flooding and erosion hazards. In recent years, the coral condition has been recorded to deteriorate in major part due to anthropogenic stressors. The effects of global warming have also been identified to contribute in part towards the recorded erosion and reduction in coral health, in the coastal environment, in Mauritius. Based on the Intergovernmental Panel on Climate Change (IPCC), the warming sea temperatures is set to further increase and impact coral health. The IPCC also predicts sea level rise of variable magnitudes for different possible climate futures.

Given the predictions of sustained reef degradation and sea level rise in the future, this report aims to contribute towards providing predictions of future wave conditions inside the lagoon area protected by a barrier and fringing reef in Flic-en-Flac, using SWAN numerical models. SWAN has a proved successful in modelling complex wave fields in coastal environments with varying bathymetries, notably for shorelines of fringing and barrier reefs (Filipot & Cheung, 2012) and along shorelines adjacent to with steep canyons (Gorrell et al., 2011)..

Problem definition

This research aims to generate estimates of the increased wave heights and added amount of wave energy which can be expected to pass over the reef under future sea level conditions, using the wave numerical spectral wave model (SWAN), at the site of Flic-en-Flac. This problem can be separated into the following research questions:

- 1- What is the current reef state and based on the IPCC predictions, how is the reef expected to evolve and how much is sea level expected to rise?
- 2- What differences are to expect in the wave heights inside the lagoon based on the mean wave climate of the area? Similarly what are the differences in wave heights and energy levels for extreme climate events?
- 3- What are the governing processes responsible for energy dissipation on the reef and are these expected to change for the sea level rise and reef condition projections?

Research Approach

The problem is approached by firstly focusing on determining the inputs of the SWAN spectral model. Requiring the definition of the present conditions and possible future state of the reef and water levels. In chapter 2, the sea level rise projections from the Assessment Report 5 (AR5) by the Intergovernmental Panel on Climate Change (IPCC) are reviewed and values are chosen based on two representative concentration pathways (RCP4.5 and RCP8.5). Also global projections of the future conditions of the reef states are reviewed. In chapter 3, a study area review covers the coastal morphology, the governing climatic processes, the tidal regime and the local coral reef condition. In chapter 4, the methodology which is carried out for both the mean and extreme climate analysis is presented. It includes the processes which were followed to acquire the site specific inputs. Chapter 5 presents the results and chapter 6 the limitation of the study. Finally chapter 7 gives important discussion points, in the form of a conclusion.

2

Literature review

2.1 Climate predictions given in the AR5 of the IPCC

2.1.1 Introduction

The IPCC (International Panel for Climate Change) was first convened in 1988 to assess scientific work in order to better understand Climate Change. Today, with more accurate climate data from satellite imagery, and a stronger network of measurement tools and sharing resources around the world; the accuracy of global weather models has greatly improved. In the most recent IPCC report, AR5 (Assessment Report 5), global SLR estimates are provided, as well as a map which allows the extrapolation of sea level change rates at specific locations. Four greenhouse gas concentration trajectories are defined in order to perform climate modeling and research; RCP2.6, RCP4.5, RCP6, RCP8.5. Each RCP defines the evolution of the greenhouse gas concentration between year 2000 and 2100.

The RCP4.5 and RCP8.5 are chosen for this analysis. For the RCP4.5 case, the greenhouse gas emission peaks around 2040 and CO₂ levels reach 540ppm by 2100. For RCP8.5 the GHG emissions increase throughout the 21st century and reach 940ppm by 2100 (IPCC, 2014), as shown in figure1.

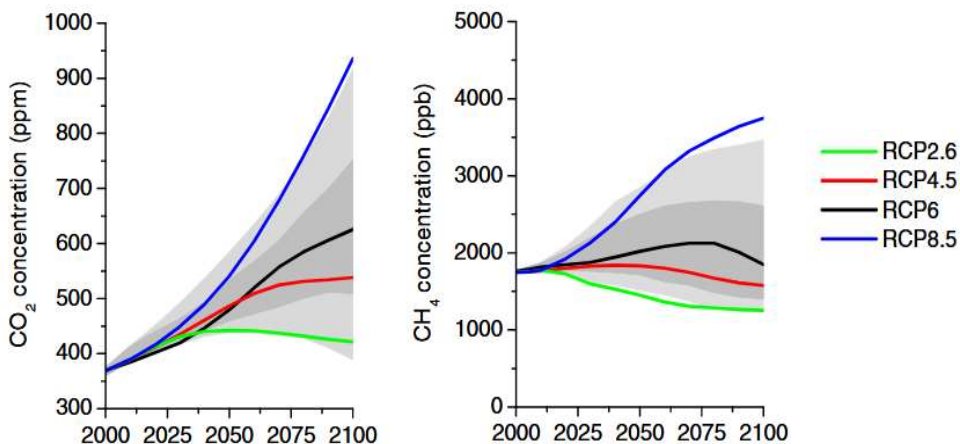


Figure 1: CO₂ emissions for the representative concentration pathways (IPCC, 2014)

The predictions for variables below describe the conditions of the future state in 2081 to 2100, relative to in the 'present condition' defined as the conditions between 1986 and 2005.

2.1.2. Sea level rise

Under both RCP4.5 and RCP8.5, sea levels are predicted to rise globally during the 21st century, following the evolution indicated in figure 2.

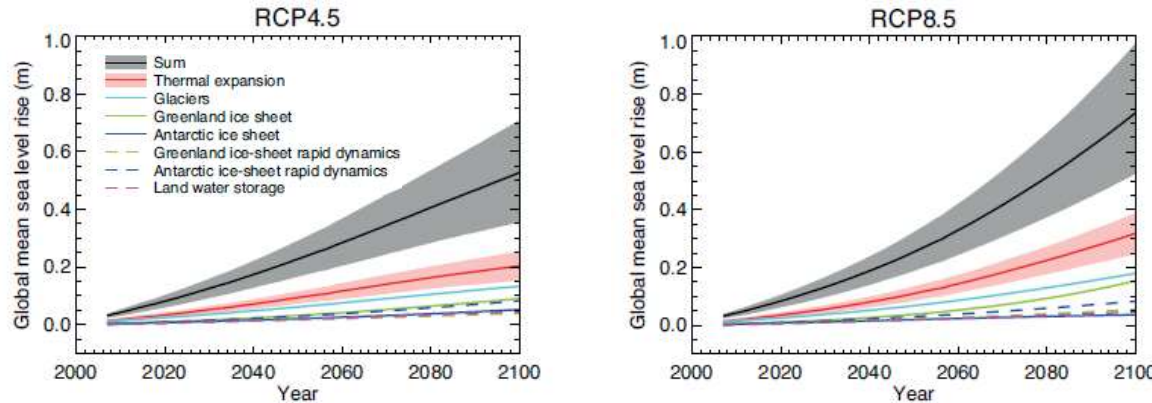


Figure 2: Projections from process-based models of (a) global mean sea level (GMSL) rise relative to 1986–2005 for RCP4.5 and RCP8.5 (Church et al., 2013)

Extraction of site specific predictions is possible using the 1°x1° grid resolution data provided from the data files of the Chapter 13 (figure 3), of the Climate Change 2013 report (Church et al., 2013).

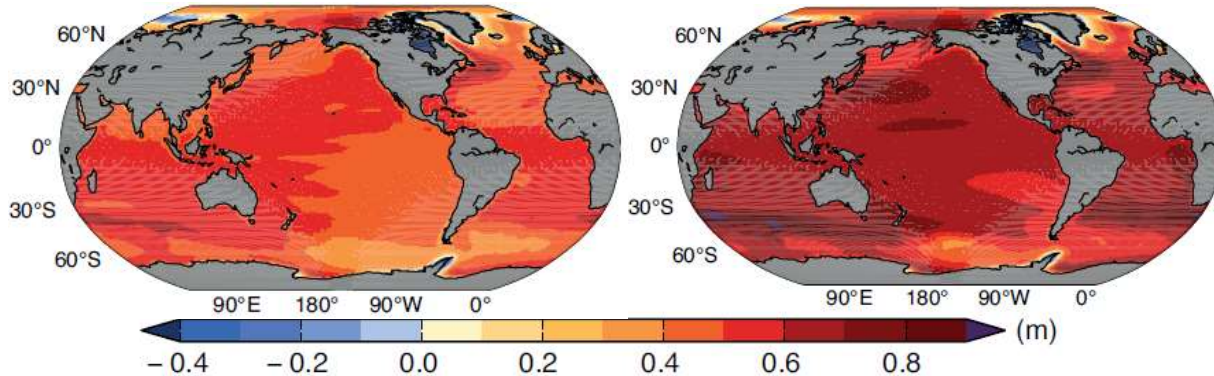


Figure 3: Mean regional sea level change (m) evaluated from 21 CMIP5 models for RCP4.5 (left) and RCP8.5 (right) (Church et al., 2013)

The mean sea water levels, at 57° East and 20° South for the interval of 2081-2100 relative to 1986-2005 are shown in the table 1. The global SLR of the upper 5% of the projections under RCP8.5 is also given in table 1.

Table 1: Regional mean seal level change (Church et al., 2013)

	Regional	Global	
	RCP 4.5	RCP8.5	RCP8.5
Mean sea level change (m) 2081-2100	0.52 [0.30 to 0.77]	0.68	0.74 [0.52 to 0.98]

2.1.3. Ocean Temperature

Much of the energy present in the atmosphere as a result of warming is absorbed by the ocean. (Shigeru et al., 2013) Temperatures in the upper 75m of the ocean have increased 0.11° per decade between 1971 and 2010 (Shigeru, et al. 2013). Under the increasing global temperatures trends predicted in the RCP4.5 and RCP8.5, superficial ocean water temperature are expected to increase further.

2.1.4. Ocean Acidity

The increase in ocean water acidity which is due to the increase of CO₂ concentration in the water causes a chemical reaction which reduces the available calcium carbonate in the water. Since coral assimilates calcium carbonate from the water to grow, the reduction of its availability limits coral growth. Also, the lower concentration of calcium carbonates can increase the dissolution and erosion of calcium carbonate from marine organisms. Other consequences of the decrease of calcium carbonate include; poorly cemented reefs, and less successful larvae settling (Wong et al., 2014).

Projections from Earth system models published in the AR5 synthesis report indicate an increase in ocean acidification in the range of 58 to 62%, and 100 to 109% for RCP4.5 and RCP8.5 pathways, respectively (IPCC, 2014).

2.1.5. Global reef survival predictions

From a global standpoint, the main source of coral cover reduction has been ocean warming (Wong et al., 2014). Acidification is nevertheless expected to increase significantly in the next decades, and combined with ocean warming, will have synergic effects on reef building capacity.

Sea level rise is a controlling factor in reef growth. Under the recent sea level rises, the coral growth has been found to be capable of matching the increasing water levels pace (Wong et al., 2014); and a number of coral species should be capable of coping with the predicted sea level increase rates predicted in 2100. Biological acclimatization may attenuate to a certain extent the coral reduction rates.

Under both RCP45 and RCP85 scenarios, coral reef will experience bleaching events of larger magnitudes and increased occurrence in the next decades. Increase in acidification will also disturb reef construction and increase erosion.

2.1.6. Wave climate variations

Due to wind speeds increase, it is likely that the annual SWH will increase in the Indian Ocean. (Church et al., 2013)

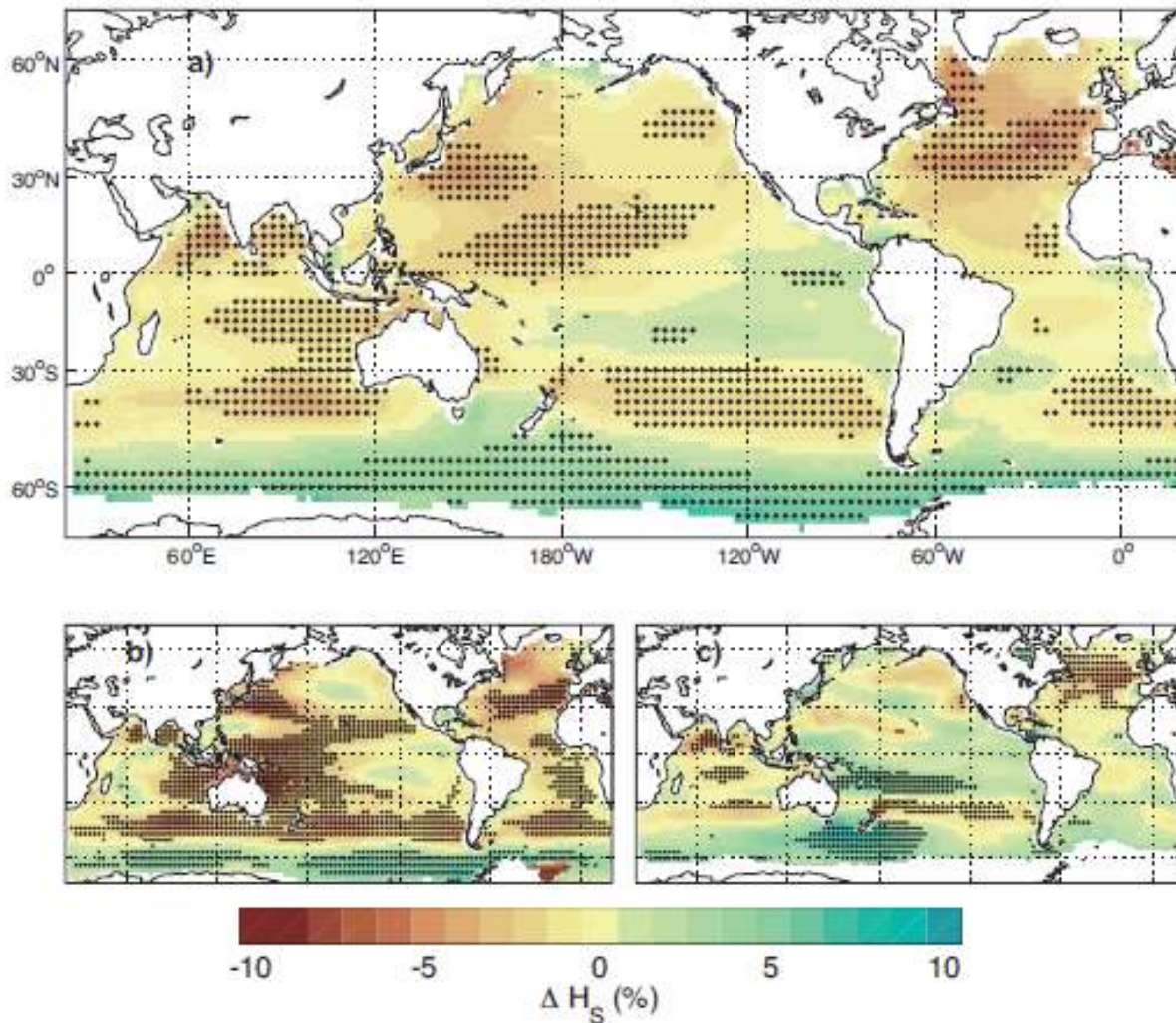


Figure 4: a) Percent change SWH between the periods of 2075-2100 and 1980 -2009, b) For months of January to March, c) for months of July to September (Church et al., 2013)

As seen from the IPCC figure 4, the significant wave height is likely to increase between 1 - 5% in the vicinity of Mauritius by 2100. Stronger winds generated from the storms during the austral

winter are predicted to be the main contributor to the SWH increase in the region. The direction of the waves generated during the winter storms correspond to the ones which would impact Flic-en-flac, on the island's west coast.

On a more recent timescale, between 1992 and 2012, Gupta et al. identify a steady increase in mean significant wave height (MSWH) and mean wind speed (MWS) in the South Indian Ocean belt, based on altimeter data (Gupta et al., 2015).

For this study, the change in SWH is only included for one scenario in the mean climate analysis. Factoring all the wave data with a coefficient may induce higher uncertainty in the accuracy of the data. An in-depth study which considers the effects of this change could nevertheless be of interest for a future analysis.

2.1.7. Cyclonic events variations

2.1.7.1. Severe storms

Extra tropical storms in the southern oceans are likely to expand their influence more poleward (Wong et al., 2014). There is low confidence that the frequency of occurrence of storms will change considerably or that the intensity of storms will change (Wong et al., 2014).

Since Mauritius finds itself on the southern oceans cyclones path, the poleward shift does not suggest much change for the island. Similarly, the projections for the frequency and intensity of extra tropical storms do not suggest that a change is necessary when modeling wave conditions under Cyclonic events, for future storm parameters relative to the present ones.

2.1.7.2. Surges

Studies in the Australia's east coast, the Gulf of Mexico, the region of New York, and India show contradictory findings in the predicted correlation between the effect of the future tropical storms and the changes on storm surges (Monismith et al., 2015). The limited number of studies as well as the contradictory findings, suggests that there is a low confidence that storm surges will change with varying storm characteristics (Monismith et al., 2015).

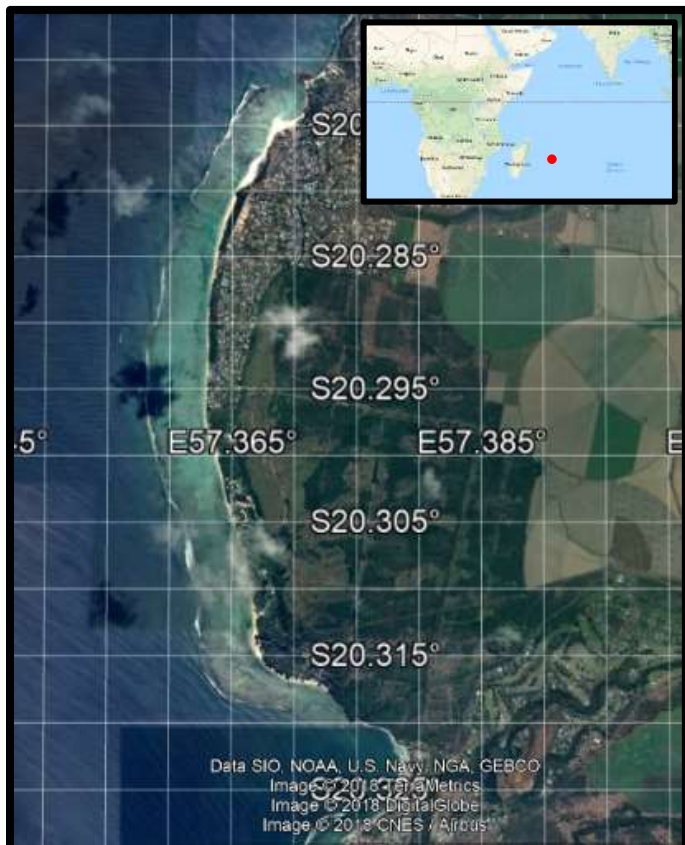
3

Description of study area

3.1 General description

The study area is located on the west coast of the island of Mauritius. The Flic-en-flac lagoon is located between the latitudes of 20.3200 and 20.2716 South, at the longitude of approx. 57.36 degrees east.

In figure 5, the Flic-en-flac lagoon appears in lighter blue shade relative to the surrounding ocean and is bordered by a line of white (waves breaking on the reef) to the west and the coast to the east.



In figure 5, the site of Flic-en-flac is chosen for this case study, since it represents a typical sandy beach in Mauritius; such that it is bounded by a lagoon extending a few hundred meters and surrounded by a fringing and barrier reef.

Flic-en-flac is one of the most visited beaches in Mauritius by both locals and tourists. Changes to the shoreline have been observed over the last decades and erosion vulnerability has been classified as high, in both erosion assessments by Baird (2003) and JICA (2015). The high vulnerability to morphological changes combined with the high use of the beach resource makes it a perfect choice for this case study.

Figure 5: Map of the study area -Flic en Flac lagoon (Google Earth, accessed on May25, 2018)

3.2 Morphology

3.2.1 General geology

Mauritius Island is located within a tectonic plate moving in a general north eastern direction. The formation of the island dates back to about 10 million years, when Mauritius was located over the almost stable hotspot presently under Reunion island (Romagnoli et al, 2015). Today, the steep slopes of the volcanic formation remains emerge from a surrounding oceanic shelf, of depths ranging within the order of 4500 to 3500 m.

3.2.2 Coastal geology

Over time, after the islands formation, coral growth in the coastal waters developed a fringing reef; with in most areas, a lagoon between the land and the main reef.

This typical cross section of figure 6 depicts the nearshore zones present in Flic-en-flac:

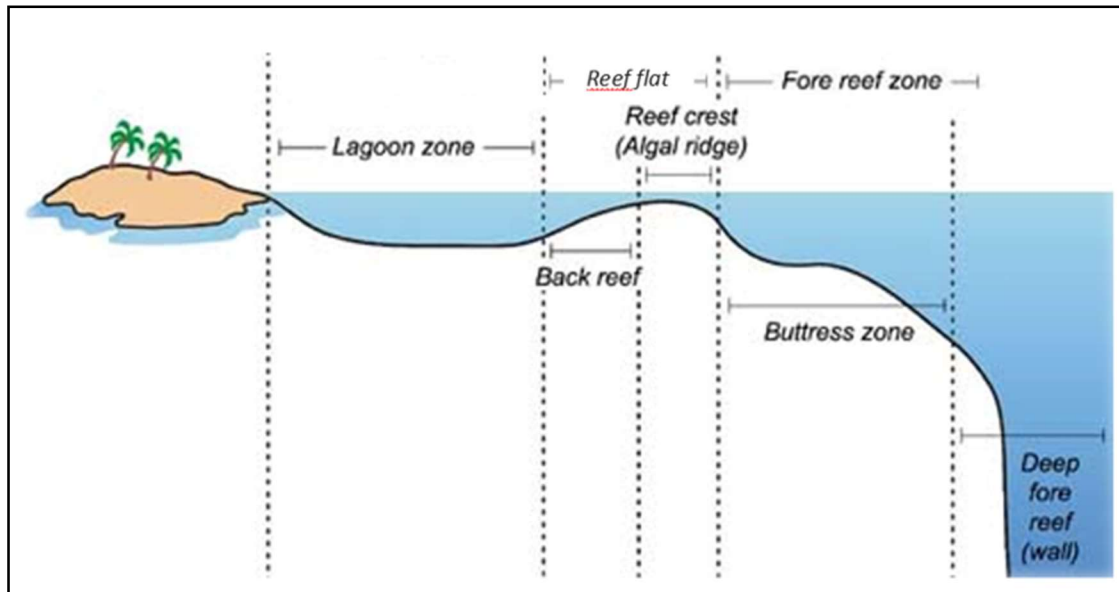


Figure 6: Typical cross section of a tropical reef (NOAA, 2017)

The lagoon of Flic-en-flac is colonized with patchy branching corals and sea grass. Sea grass is located across from sources of fresh water, and patchy corals are found north of the pass, in the lagoon facing Villa Caroline hotel, in the bay at the north end of the lagoon, in front of la Pirogue Hotel (Baird, 2003). The seabed present at the majority of the lagoon is comprised of sand veneer laying over calcareous substrate from past reef growth. The predominant coral species inside the lagoon are porites. The most common sea grass species is *Syringodium isoetifolium* followed by *Halodule uninervis* (Baird, 2003).

The fore reef and reef flat were noted to have a poor coral cover. The MMCS report (MMCS, 2010) estimates live coral between 5 and 50% with on average about half of corals to be of the 'massive

coral species', and less than 25% to be branching corals. A pass in the reef exists approximately at latitude 20.290, and a number of false passes are also present. The buttress zone extends from the reef flat to approximately 20m below sea water level.

3.3 Reef as a sediment source

3.3.1 Sediment source

The sediments of the Flic-en-flac beach, like most tropical beaches are composed of calcium carbonate particles. A portion of the sediments originate from the coral breaking down into small particles from wave and current action. Certain species (sea urchins and fish) graze the live coral, releasing fine coral derived sediments. Some of the calcium carbonate input comes from shell or other fauna remains, such as bivalves, molluscs, sea urchins. Algae is also a source of sediments, notably from the breakdown of the binding surface of the red algae or the secretion of fine particle calcium carbonate from green algae (*Halimeda*) into the water column (Baird, 2003).

3.3.2 Energy dissipater

The barrier reef serves as a natural breakwater as it dissipates the incoming energy through wave breaking and friction processes. As stated in the impact of sea level rise paper by Ragoonaden, (1997) the coral reefs surrounding the lagoons in Mauritius dissipate close to the entirety of the wave energy.

3.4 Wave climate of Mauritius

3.4.1 Climatic systems, winds and resulting waves

The wave climate in Mauritius is governed by its location in the southwest of the Indian Ocean. This subtropical region is subject to three main climatic processes which generate waves: 1- the trade winds, 2- the southern storms and 3- cyclones.

- 1- Trade winds: The quasi-permanent high pressure system in the Indian Ocean generates constant south easterly winds and waves throughout the year. Wind speeds vary from 5m/s to 25m/s from June to September, (Dhunny, Lollchund, & Rugoophuth, 2015) forming waves of typical peak periods in the order of 12s (Baird, 2003).
The location of the high pressure system relative to Mauritius (see figures 7 and 8) at different times of the year, explains the stronger winds experienced in the austral winter and weaker in the austral summer.
- 2- Southern storms: The low pressure systems to the south of Africa travel from west to east. Unobstructed by land, the fetch over which the storms blow results in waves of high peak period and wave height. Swell reaching the island approaches from south westerly to southerly directions. As seen on figure 7 and 8, the southern low pressure system shifts

from a more south to more north location in the austral winter; resulting in stronger and more frequent swell events in Mauritius during that time.

- 3- Cyclonic events: During the months of summer, when the trade winds become more unstable, and convective instability develops, cyclones may form in the Southern Indian Ocean. These typically form to the north east or north west of the Island, before their trajectory dips in a southerly direction. Waves from these episodic events generally approach from a northerly direction. As the extra-tropical storm displaces towards lower latitudes, higher waves are felt on the east or west coast, depending on the cyclones trajectory.

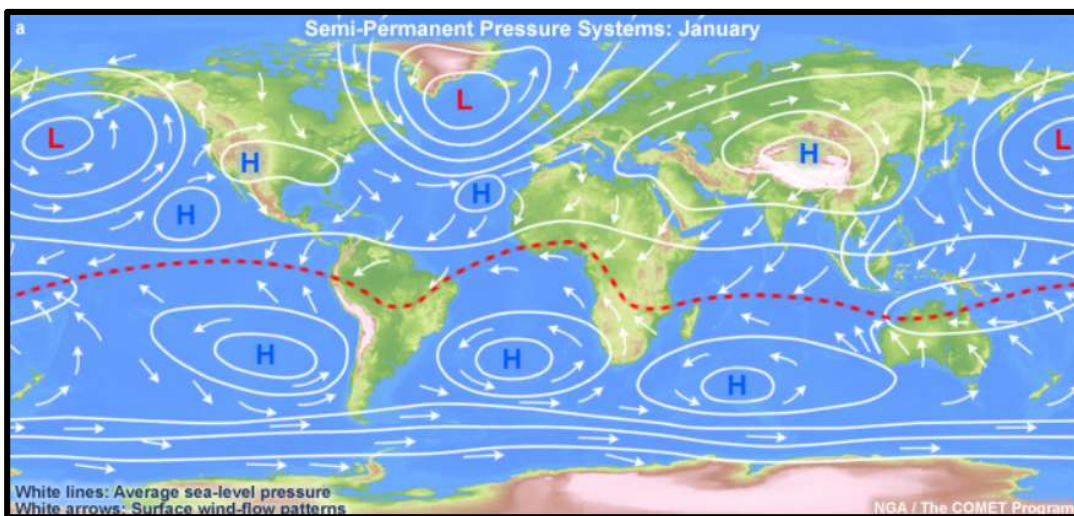


Figure 7: Global pressure systems during the austral summer (NCAR, 2011)

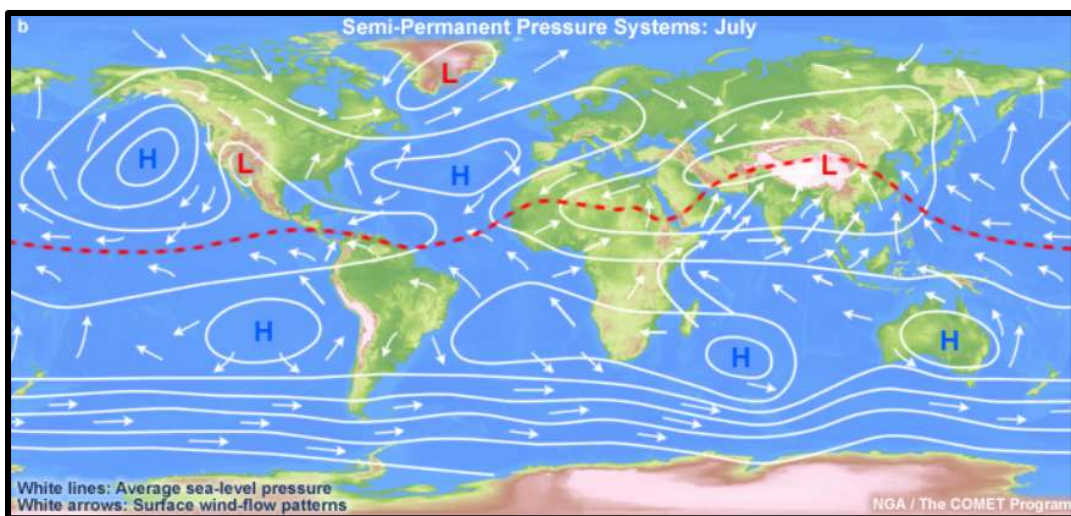


Figure 8: Global pressure systems during the austral winter (NCAR, 2011)

The west coast of Mauritius, where Flic-en-flac is located, is subject to waves from the southerly storms and may be affected by episodic cyclonic waves, depending on the cyclones' trajectory. The waves generated by trade wind do not affect Flic-en-flac significantly.

3.4.2 Wave climate data available

3.4.2.1 ECMWF - EraInterim

The European Centre for Medium-Range Weather Forecasts (ECMWF) is an independent intergovernmental organization which produces climatic data to improve current forecasts and to better scientific research. Forecasts and climate reanalysis data is available from their website for academic uses.

The Era-Interim atmospheric reanalysis data uses available observations with prior information from the model forecast to estimate the global state of the atmosphere (Shigeru et al., 2013). This atmospheric data covers a continuous timespan from 1979 to today, and generates data for a $0.75^\circ \times 0.75^\circ$ spatial resolution. Ocean waves parameters include: mean wave period, mean direction, significant wave height and are available in intervals of 6 hours. The significant wave height is calculated from the two dimensional wave spectrum. The mean wave direction is taken as the mean of all directions over all frequencies of the spectrum, and the mean wave period is deducted from the reciprocal integral moment of the frequency wave spectrum.

3.4.2.2 EraInterim wave data limitations

In a past analysis Naseef & Kumar (2017) compare EraInterim reanalysis data and wave buoy data records and conclude that the extreme wave climate derived from EraInterim is significantly smaller than the one derived from wave buoy data. Indeed, EraInterim data misses certain wave height values, since the record interval is of 6hrs, compared with buoy data record interval of 30min. As EraInterim takes the average of the record within the 6hr window, there is an additional damping effect. Similarly, due to the damping effect, we would expect the wave minimums to be over-estimated in Era-interim data. When considering extreme wave conditions, the exclusion of one wave may result in a large difference in 100year return Hs value (Naseef & Kumar, 2017). The cyclonic wave climate is highly variable due to the cyclones' unpredictable trajectory, as well as the variable wind intensities throughout their lifespans, making it even harder to accurately represent the peaks with 6hrs interval data. The significant wave height from wave buoy data acquired from the northeast coast of Mauritius was compared with EraInterim data during cyclonic events. At first glance, similar to Naseef & Kumar (2017), the Era-Interim data underestimates the SWH of the extremes. See Appendix A.1.

3.5 Tidal regime

The tides in Mauritius are of relatively low amplitude (Micro-tidal) and are mainly a semi-diurnal. The neap range and spring range are 0.3m and 0.5m, respectively. The range from the lowest to highest astronomical tide is 0.8m (Baird, 2003) and the ratio between the principal lunar semidiurnal tide constituent (M2) and the principal solar semidiurnal component (S2), is 0.64 (Lowry, Pugh, & Wijeratne, 2008). The mean tidal levels are high from January to March and low between May and October (JICA, 2015). Figure 9 represents the tides for the months of May and June 2018 based on forecast data from the Mauritius Meteorological Services (2018).

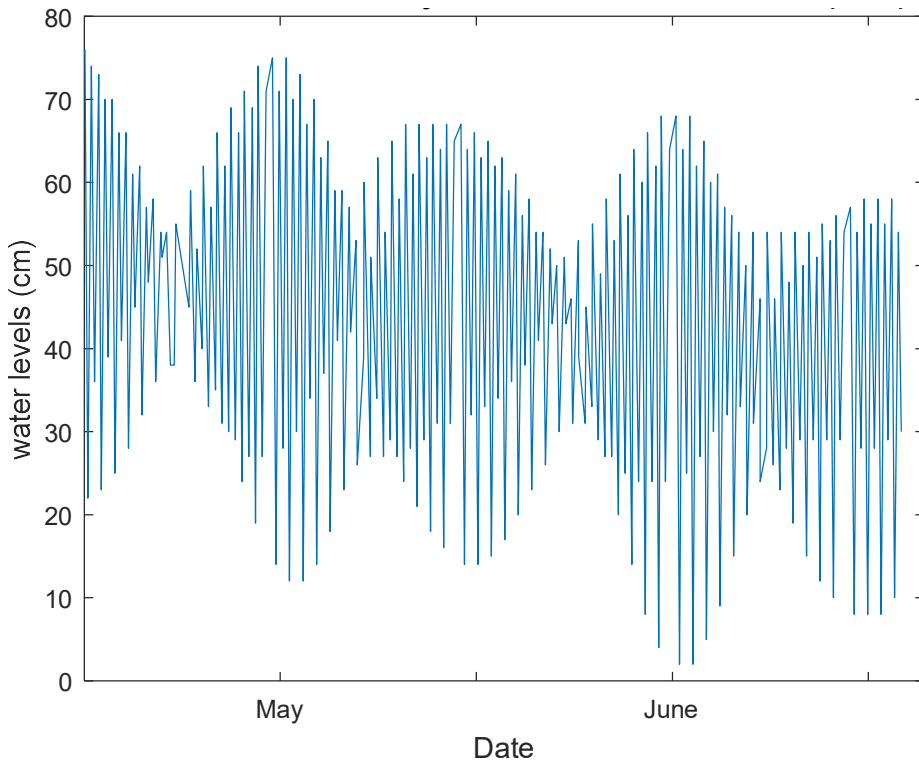


Figure 9: Tidal variations over May and June 2018, in Mauritius (ACD)

The height of tides is taken from the Admiralty Chart Datum, which is the mean of the average lowest tides recorded in Port Louis.

3.6 Sea Level Rise

3.6.1 Global Historical sea level rise

The Global sea levels have risen approximately 120 meters between the last glacial maximum (25000 years ago during Pleistocene) and 2000-3000 years ago (figure 10). The sea levels have since been relatively constant, (Kristensen et al., 2007), with rates of change within the order of the tenth of mm/yr.

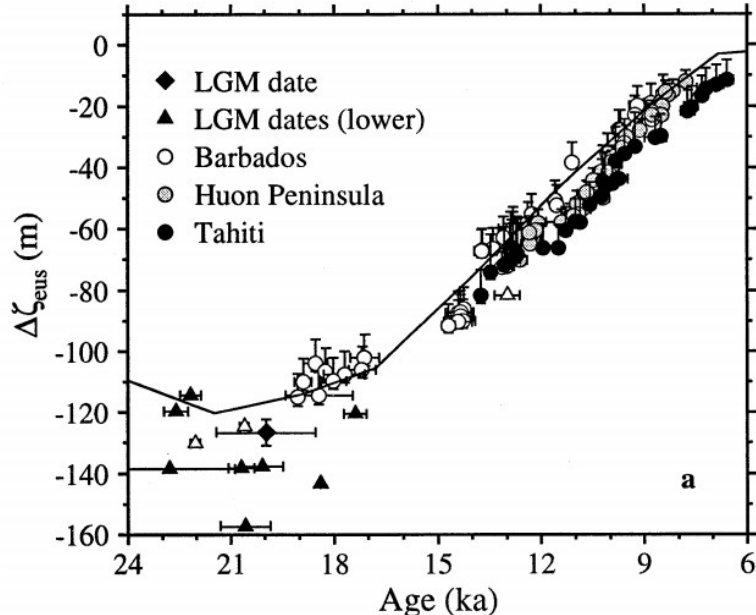


Figure 10: Sea level change from the last glacial period based on sites in different global locations (Fleming et al., 1998)

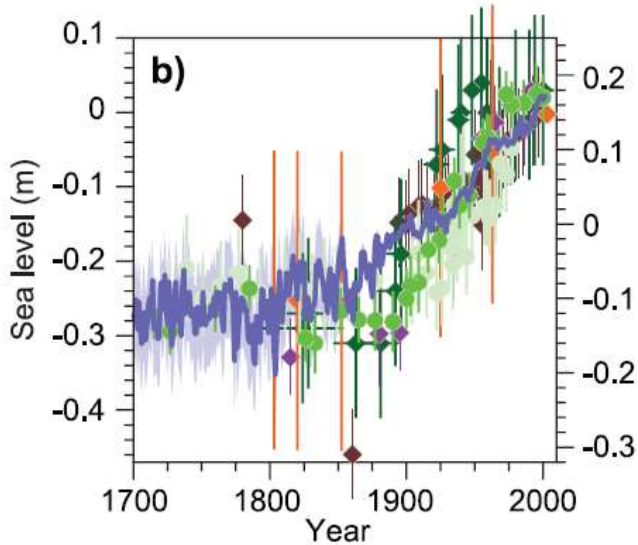


Figure 11: Sea level rise at different worldwide sites and from tide gauge reconstructions (Church et al., 2013)

Given a timescale of a few centuries, the sea level change rates have increased by an order of magnitude since the 1700s, from tenth of millimeters per year to millimeters per year (Gehrels & Woodworth, 2013), as can be observed in figure 11.

3.6.2 Recent Sea level rise trends in Mauritius

Fitting a linear line to the yearly average water levels of the 31 years of tide gauge data (Holgate, et al., 2013; PMSL, 2018) from the Port Louis station show a 4.8 mm/yr rate of local increase in local sea levels, plotted in figure 12. Since the IPCC AR5 predicts a global sea level rise between 1993 and 2010 at 3.2 mm/yr, we note that the local rates are slightly higher although within close range of the global projected rates.

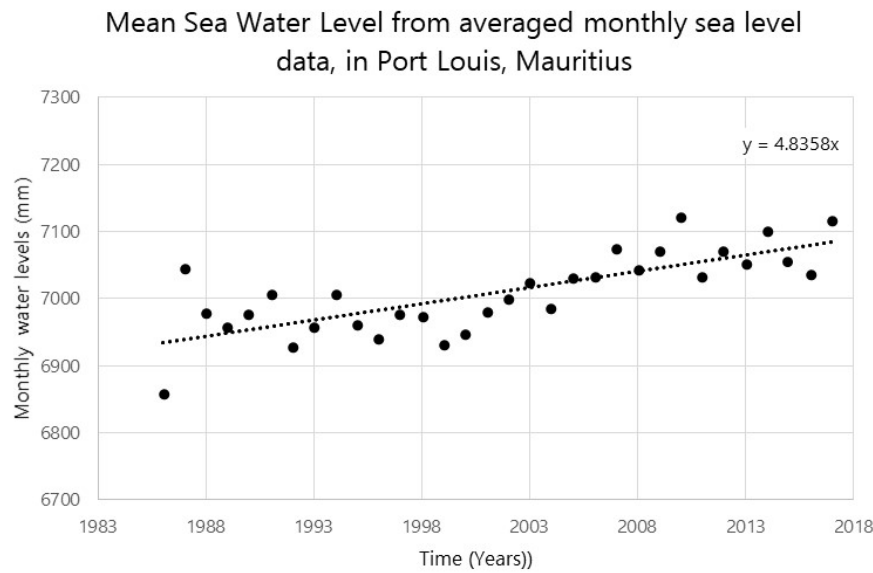


Figure 12: Trend of average sea levels in Mauritius (1987-2017)

3.7 Current state of the Flic-en-Flac coral barrier and fringing reef

Coral reef health is subject to natural and anthropogenic threats. Cyclonic events are natural causes which can result in reef degradation. In Flic-en-flac, studies suggest that the main causes of degradation are nevertheless anthropogenic. These include:

- a- The increase of freshwater input into the lagoon after rainfall. Due to residential developments about a kilometer inland from the beach, coastal wetlands are filled. Drainage through percolation which would take place at a slow rate through the wetland towards the sea, is modified to drainage into the lagoon through one canalized channel. This resulted in the loss of several square meters of patch reef, and the successive growth of sea grass patches in areas fronting the inlet (Baird, 2003);
- b- A number of hotels have carried out lagoon alterations to improve bathing conditions in order to provide better accessible touristic use, predominantly by clearing coral patches. This occurs notably in the vicinity of the Mauriplage Hotel, Sugar Beach Hotel and la Pirogue Hotel (Daby, 2003).
- c- Coral bleaching from higher water temperatures;
- d- Siltation in the lagoon, discharge of fertilizers and effluents in the lagoon.

Reports from JICA (2015), Baird (2003), and MMCS (MMCS, 2010) describe in various levels of details the conditions and the evolution of the reef health in Flic-en-flac over the last couple decades.

- 1- In the lagoon, the patch corals identified inside the lagoon showed 5% to 38% of live communities. The transect measurements noted a coral cover of the reef of 30% at Wolmar, and 40% in front of the Bay at Villa Caroline. And the coral cover of the spur and groves of fore reef was noted to be poor with less than 10% of coral cover at 10m (Baird, 2003).
- 2- The MMCS report indicates the live coral on the reef at 30 to 50% for about half of the barrier. On the remaining portions the live coral cover ranges between 5 and 30% (MMCS, 2010)
- 3- The JICA (2015) report indicates that the reef in Mauritius as a whole has evolved from an average coral cover of 50% across the reefs in 1998 to 25% in 2010. The evolution noted suggests a decline of the Mauritian coral cover on the long term.

Based on the above mentioned reports, a live rate of no more than 25 to 30% may be assumed for the purpose of modeling in this study.

[3.8 Projections of the future state of the reef in Flic-en-flac \(1986-2100\)](#)

The coral reef growth rates Mauritius have been capable of matching the sea level rise in the past. Indeed, during and post the Holocene transgression, the reef vertical growth is believed to have matched the SLR, with rates of 1.5 to 90mm/year in Mauritius (Baird, 2003). Baird (2003) identifies *Acropora Formosa* as the most common coral throughout lagoons in Mauritius while porites inside the Flic-en-flac lagoon. A coral transplant study in Malaysia, records growth rates in the order of $0.55 \pm 0.13 \text{ cm mth}^{-1}$ for *Acropora Formosa* on the reef (Xin et al, 2016), while growth rates of porites, studied in Indonesia indicate that they are within a range of 0.8 – 1.2 cm/year (MMCS, 2010). The coral growth rate capability of the currently dominant coral specie in Flic-en-flac and the other lagoons of the island may physically be capable of following the growth rates matching the SLR under the IPCC prediction scenarios.

If the reef continues to deteriorate at the rate it has been over the last decades, it seems probable that there will be very little to no live reef by 2100 in Flic-en-flac, unless drastic changes occur. Under circumstances where the anthropogenic stresses are reduced; the coral will most probably still face increased degradation as suggested by the IPCC AR5 report, due to the increase in water temperatures and acidity levels.

4

Methodology

In this study the wave height variations in the lagoon of Flic-en-flac are considered for different scenarios under two different types of wave climates:

- 1- The mean wave climate – governed by the southern storms (See 3.4.1),
- 2- The extreme wave climate – governed by extra-tropical storms (See 3.4.1).

4. 1 Model set-up – Mean Wave climate

4.1.1 Procedure

The mean wave climate was modelled under 8 different scenarios. Each scenario includes a sea level and reef friction factor based on the actual or projected case considered (See 4.12).

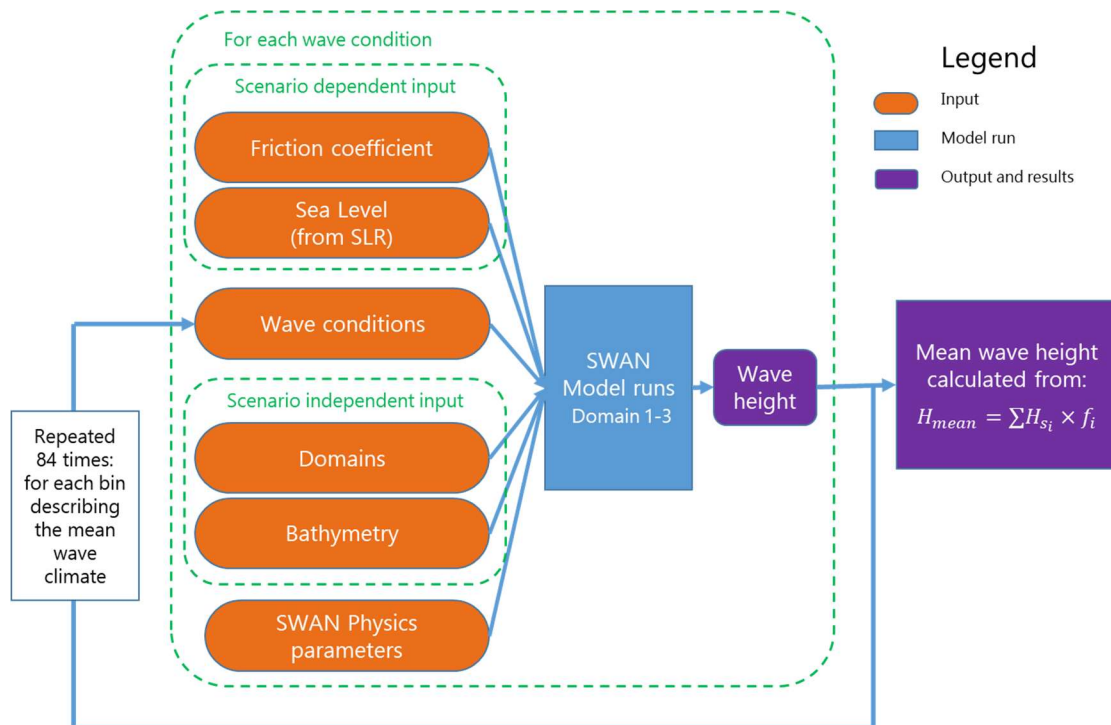


Figure 13: Flowchart of the procedure followed for each mean wave climate scenario

For each scenario, all the filtered wave conditions representative of the mean wave climate were run in SWAN. Other than the wave parameters, including: the SWH, the period, and the direction; the SWAN scripts were kept the same for the model runs of every wave condition. Only in Scenario 7, the wave heights and periods were increased. The flowchart in figure 13 shows the procedure followed.

4.1.2 Scenarios – mean wave conditions

The different wave conditions representing the mean wave climate susceptible of affecting Flic-en-flac were run in SWAN under the scenarios presented in table 2.

Table 2: Mean wave climate scenarios

Scenario	Abbr.	Description	Present vs Future	SLR projection	Reef conditions	Water level relative to MSL (m)
Reference	Ref	Present conditions	Present	N/A	Current	0
Scenario 1	Sc1	Future conditions under RCP4.5 (1985-2100)	Future	RCP4.5 (Reg. mean)	Low survival	0.52
Scenario 2	Sc2	Future conditions under RCP8.5 (1985-2100)	Future	RCP8.5 (Reg. mean)	Low survival	0.68
Scenario 3	Sc3	Future conditions under upper 5% projections RCP8.5 (1985-2100)	Future	RCP8.5 (up. limit)	Low survival	0.98
Scenario 4	Sc4	Present conditions - with a dead reef	Present	N/A	Current	0
Scenario 5	Sc5	Present conditions - with the highest astronomical tide	Present	N/A	Current	0.4
Scenario 6	Sc6	Future conditions under RCP4.5 – with non-growing reef but of maintained roughness	Future	RCP4.5 (Reg. mean)	Current	0.52
Scenario 7	Sc7	Future conditions under RCP4.5 – with 5% increase in wave heights	Future	RCP4.5 (Reg. mean)	Low survival	0.52

No scenario was modelled to represent the optimistic outlook of the reef surviving with a vertical growth matching the SLR rates. Under those assumptions, little wave parameter changes are expected relative to the reference conditions.

Based on the predictions of the reef health in Flic-en-flac, discussed in section 3.8; scenarios 1-3 assume a low coral survival, and no growth over the current reef height. Friction coefficients used were reduced to the one of a smooth rock. To evaluate the effect of the friction coefficient, scenario 4 is a replica of the reference run, with a lower friction coefficient corresponding to the one of a dead reef. Similarly scenario 6 and scenario 1 differ only in their friction coefficients. Scenario 5 presents the current conditions under the highest astronomical tide, to provide a sense of the range of wave height protruding into the lagoon. Scenario 7 assumes a SLR according to the mean RCP4.5 projections, and also includes a wave height increase suggested by the IPCC. This scenario will be compared with scenario 2.

4.1.3 Choice of location of EraInterim data retrieval

The wave data used for the mean wave climate analysis was retrieved at coordinates of 56.25° E and 22.5°S (See Appendix B5). The decision to use data from a location south west of Mauritius are based on 2 main reasons:

- As discussed in section 3.4.1, the wave climate in Mauritius is a result of two main wind systems (trade winds and the southern storms). It is therefore very common to encounter waves approaching from both directions simultaneously. The EraInterim data only provides a single mean wave direction, and therefore, in the case of simultaneous wave approach, one wave direction will be overshadowed and not represented. Using wave data south west of Mauritius reduces the noise from the trade wind waves and provides a better representation of the proportion of south westerly swells which will reach Mauritius.
- Reunion Island shelters Flic-en-flac from much of the waves which travel from the south west. The spatial resolution of Era-Interim is too large to accurately represent the wave transformations which take place when southwesterly waves approach Reunion Island. Since in the model the wave is input on the computational boundary, broadening the model surface south of Reunion enables to account for the reflection, diffraction and shoaling in the SWAN model.

Given the wind speed and direction between the data extraction point (56.25°E and 22.50°S) and Mauritius, minimal wave growth is expected, based on wind data from EraInterim. (Appendix B1).

Wave Rose from EraInterim data [56.25°E 22.5°S]

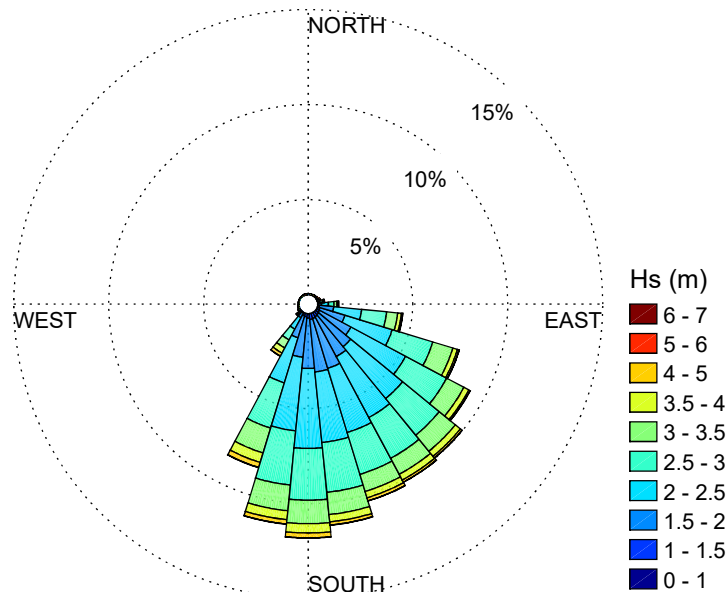


Figure 14: Wave rose based on 39 years of EraInterim data

In order to best describe the wave climate at site, the data was retrieved for the longest available period of 39 years, between 1979 and 2017. Figure 14 shows the corresponding wave rose.

4.1.4 Wave input

The wave data from Era-Interim was sorted into directional intervals; and tables of frequencies of occurrence were deduced for SWH and period bins of 2 seconds and 1 meter, respectively. A large sorting interval for the period and the wave height was chosen to restrict the number of runs to a manageable number. Furthermore, conditions noted to occur less than 2hr/year were not considered for the model. Waves of mean direction smaller than 163.125° were also discarded, due to the limited effect these conditions would have on the study area. Figure 15 shows the interval of wave directions considered for the mean climate runs.

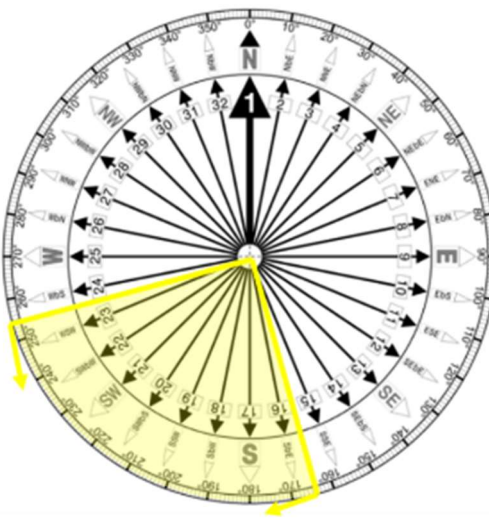


Figure 15: Interval of mean wave directions considered for the SWAN runs

The wave direction, SWH and mean period input used in the SWAN model corresponds to the median of the bin range for each parameter. The cumulative frequency of occurrence for all the conditions modelled in the analysis sums to a total of 45.39% of the total waves recorded in the wave climate data. In table 3, all the wave conditions used for the mean climate runs are listed. Tables of the frequencies of occurrence of the chosen wave bins are shown in the Appendix B.2.

Table 3: List of the wave inputs including the swh, period and wave direction (Nautical convention) for all runs performed in scenarios 1 – 6.

Direction	SbE 168.75 °	S 180 °	SbW 191.25 °	SSW 202.5 °	SWbS 213.75 °	SW 225 °	SWbW 236.25 °	WSW 247.5 °
Significant wave height (m) - period (s)	1.5m 7s	1.5m 9s	1.5m 9s	1.5m 9s	1.5m 9s	1.5m 9s	1.5m 9s	2.5m 9s
	2.5m 7s	2.5m 9s	2.5m 9s	2.5m 9s	2.5m 9s	2.5m 9s	2.5m 9s	2.5m 9s
	1.5m 9s	3.5m 9s	3.5m 9s	3.5m 9s	3.5m 9s	2.5m 11s		
	2.5m 9s	4.5m 9s	1.5m 11s	1.5m 11s	1.5m 11s	3.5m 11s		
	3.5m 9s	1.5m 11s	2.5m 11s	2.5m 11s	2.5m 11s	2.5m 13s		
	4.5m 9s	2.5m 11s	3.5m 11s	3.5m 11s	3.5m 11s			
	1.5m 11s	3.5m 11s	4.5m 11s	4.5m 11s	4.5m 11s			
	2.5m 11s	4.5m 11s	2.5m 13s	2.5m 13s	2.5m 13s			
	3.5m 11s	2.5m 13s	3.5m 13s	3.5m 13s	3.5m 13s			
	4.5m 11s	3.5m 13s	4.5m 13s	4.5m 13s	4.5m 13s			
	2.5m 13s	4.5m 13s				3.5m 15s		
	3.5m 13s					4.5m 15s		
	4.5m 13s							

4.1.4.1 Wave input – Scenario 7

In scenario 7, the effects of the increase in the SWH predicted by the IPCC AR5 is considered. The bin average wave height used for modelling (shown in table 3) is multiplied by a factor of 1.05, to represent the 5% increase in wave height. To account for the resulting changes in periods, a relationship between the SWH and the mean period is plotted in figure 16.

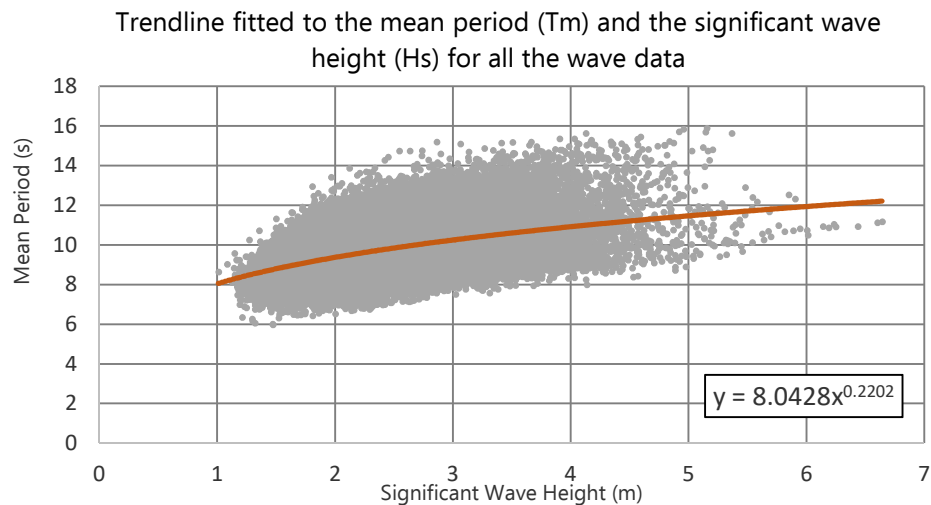


Figure 16: Graph showing the relationship between the mean period and wave height

An equation of the type $y=ax^b$ was found to describe the correlation between the mean period and the wave heights for all the data.

$$H_s = 8.043 T_m^{0.2202}$$

First, with the median period of each bin (tables in Appendix B.2) corresponding wave heights were deduced from the equation fitted equation. This wave height was increased by 5% and the equation was used again to calculate the new period (for bin medians 9-15s). In table 4, the new wave periods used for scenario 7 are indicated.

Table 4: Table of the modified wave heights and periods, for a SWH increase in Sc7

Period of bin median (s) (Sc1-6)	7	9	11	13	15
	↓	↓	↓	↓	↓
Converted mean period (s) (Sc7)	7.07	9.10	11.12	13.14	15.16

4.1.5 Model domains

The SWAN simulations were run in three nested grids with decreasing mesh sizes. The outer domain boundary input was taken from EraInterim data. The results of computation over the outer grid, defined the input for the inner grids. The largest model domains' (Domain 1) boundaries extend from 20.2°S to 21.6° S and 55.4° E to 57.4° E. The southernmost boundary was chosen to include Reunion Island, to ensure the refraction and diffraction of southwesterly waves are taken into account. A coarse resolution of the computational and bathymetric grid of 0.005° by 0.005° was used, in the longitudinal and latitudinal directions respectively. The second domains (Domain 2) grid was reduced to 0.00075 by 0.00075° length cells, and includes the southwest portion of the Mauritian coast, to account for wave transformations the waves approaching the nearshore. The rectangular boundary's coordinates are 20.22° S to 20.52° S and 57.23° E to 57.38° E. The third and most refined grid has cell sizes of 0.00016° in the longitudinal direction and 0.0002° in the latitudinal direction. This roughly equates to 18m x 22m. Domain 3 extends between 20.265° S to 20.325° S and 57.340° E and 57.38° E. In figure 17 the three domain extents are shown.

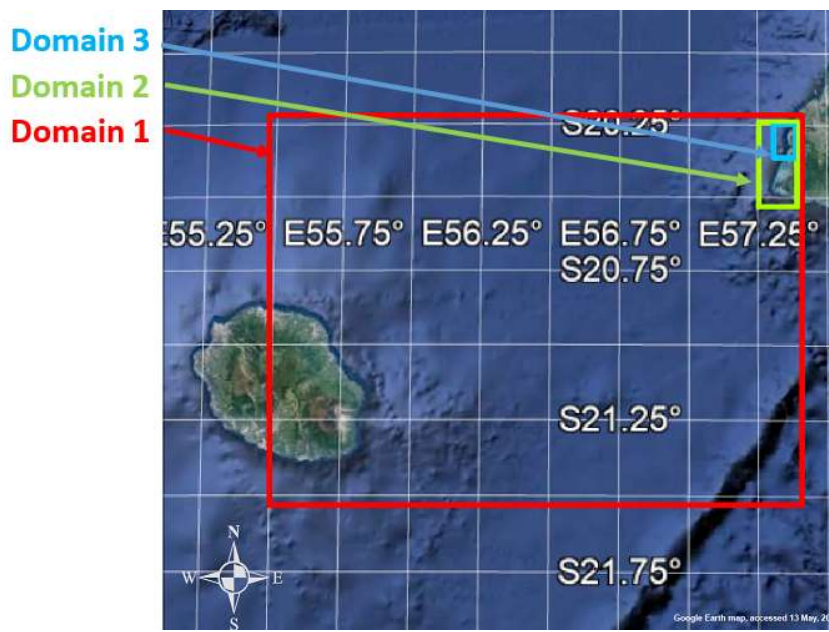


Figure 17: Computational boundaries of SWAN domains

4.1.6 Bathymetry

Limited bathymetric data is available for the coastline of Mauritius. Freely available navigational charts (Navionics) and some hard copy maps provided from the MOI (Mauritius Oceanography Institute) of the lagoon of Flic-en-flac were used to recreate a bathymetric surface to use as input in the SWAN models.

ArcMAP10.5 was used to digitize depth point data values from the navigational charts and the Flic-en-flac maps. Interpolation between the depths of the input the data points enabled creation of a bathymetric surface. Carrying out this process induces some inevitable estimation error, of different levels depending on the technique used. The geostatistical kriging interpolation method has proven to keep bathymetry interpolation errors within a low range (Ineda, Uis, & Tefanoni, 2007), notably in areas of steep bathymetric changes such as in the south west coast of Mauritius. See Appendix B.3 for a map of the created bathymetry from which depth data points were extracted.

The depth of the reef flat was assumed at -0.3m below the LMSL. This assumption is founded on the reef being exposed during the lowest spring tides (Daby, 2003) and based on the JICA (2015) report. No reef crest was modelled, due to limited data. Although local variations and a finer detail resolution was built in ArcMap10.5, the cross section shown in figure 18 represents a theoretical typical section of the 3D bathymetry generated.

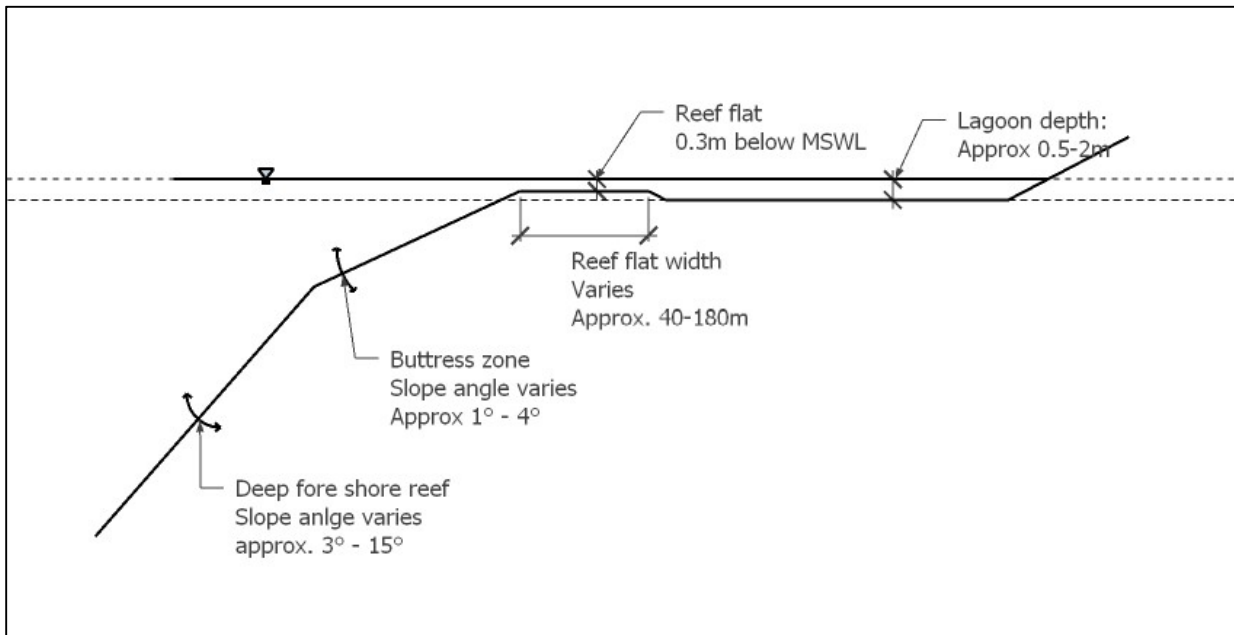


Figure 18: Reef cross-section representing the typical bathymetric dimensions

The buttress zone typically slopes gradually for about 150 m to depths around 5m, where cliffs of 12 m and more are noted (Baird, 2003).

4.1.7 Tide input

Given the wave data available, the joint probability of the tides and wave conditions are unknown. To ensure consistency in the SWAN models, the runs were done in a stationary mode at the Local Mean Sea level (LMSL) for all cases.

4.1.8 Friction

The bottom friction contributes towards damping wave energy traversing the reef. To account for it, a friction coefficient relates the orbital wave velocity and the bed shear stress. The bed induced friction is nevertheless highly variable in space and time, especially in highly heterogeneous and complex environments such as reefs. Reef surface morphological characteristics vary with the type, the density, the structural complexity and distribution of coral. Friction coefficients (f_w) are typically deduced from measurements of bed shear stress or energy loss over a given distance (Osorio, 2017).

Based on a study of the reefs in the Seychelles, Sheppard et al. (2005) estimates (f_w) = 0.1 for a smooth coral pavement and (f_w) = 0.2 for a healthy coral reef. Quataert et al. (2015), reports friction coefficients of (f_w) = 0.3, from a field data for the fore reef at Roy Namur, in the Marshall Islands. Some studies report a higher friction coefficient, in reefs of higher complexity; such as (f_w) = 0.6 and (f_w) = 1.8 at the Ningaloo reef (van Dongeren et al., 2013) and the Palmyra Atoll (f_w = 1.80) (Monismith et al., 2015).

In this study, the choice of the friction coefficient is estimated based on Flic-en-flacs' predicted reef health, and the above mentioned friction coefficients published for reef environments; given the assumption that the healthier a coral reef, the higher the structural complexity. The selected friction coefficients are indicated in table 5.

Table 5: friction coefficients for different coral conditions in Flic-en-flac

Friction coefficients	Current coral condition	Dead coral
Reef flat	0.25	0.1
Fore-reef – Buttress zone	0.25	0.1
Lagoon	0.15	0.1
Deep fore reef	0.1	0.1

4.1.9 SWAN parameters

Table 6: SWAN parameters used

SWAN parameters	Value	Included in Domain		
		1	2	3
<i>Wave breaking parameters</i>		x	x	x
γ	0.94			
B	1.09			
<i>Wave input</i>		x	-	-
Jonswap	3.3			
<i>Diffraction</i>		x	x	-
Coefficient	1			
<i>Friction</i>		x	x	x
Madsen	Variable			
<i>Setup</i>	default	-	-	x

The default Jonswap ($\gamma=3.3$) spectra was used as input for the southwesterly swell. The depth induced wave breaking parameters used were chosen according to Filipot & Cheung, (2012) Findings in their study relating to SWAN models in reef like environments calibrated using laboratory experiments and field observations. The chosen breaking parameter γ is also within the computed range of 0.84 ± 0.21 determined in a SWAN model calibrated to the Palmyra Atoll reef (Monismith et al., 2015). Since the winds in the domain are predominantly from E to ESE, wave generation was considered negligible. Whitecapping was also considered negligible since it is closely related to the wind (Holthuijen, 2010). Frequency and directional bins were defined by 24 logarithmically spaced intervals between 0.05 and 1 Hz. The direction was discretized into 36 bins spaced 10° . A summary of the parametrizations used in the SWAN model is given on table 6. A breakdown of certain key equations used in SWAN are presented in Appendix B.6. For further information please refer to the SWAN scientific and technical documentation (Swan, 2009).

An Example of the SWAN script for every domain used is found in the Appendix B.4.

4.2 Model set-up - Extreme wave climate

4.2.1 Procedure

For the friction coefficient assumptions, the SWAN parameters and the bathymetry refer to chapters 4.1.6, 4.1.8 and 4.1.9. The results of each extreme climate runs are the output of one model run. The procedure followed to simulate each extreme event is schematized in figure 19.

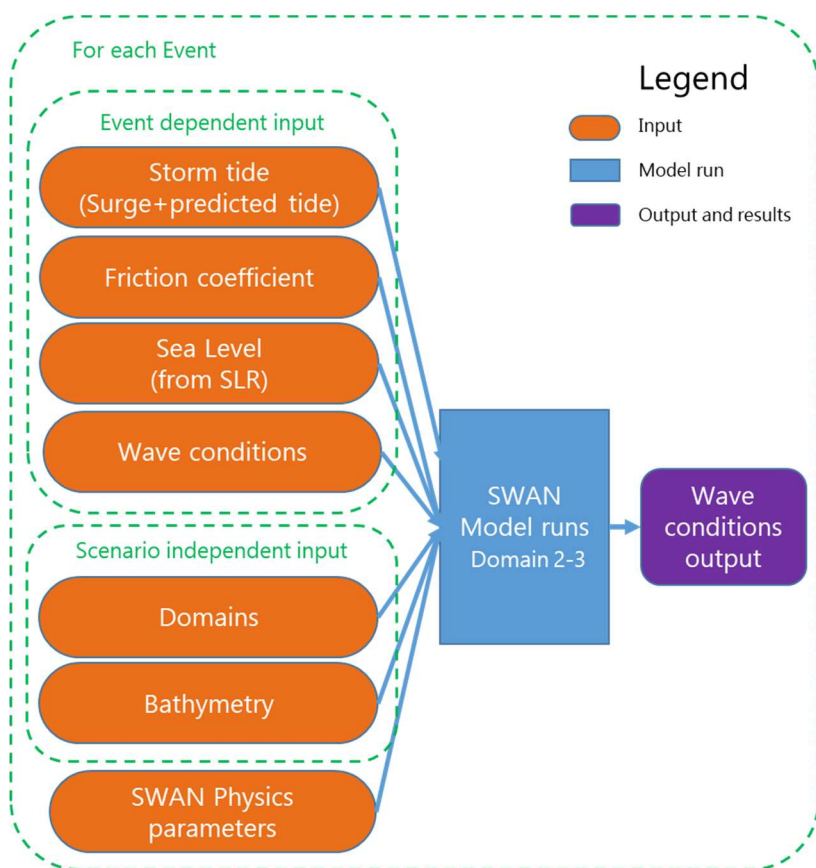


Figure 19: Flowchart of the procedure followed for each Event

4.2.2 Scenarios – Extreme wave climate

Extreme climate scenarios are referred to as events, to differentiate the wording with the mean climate cases. Wave climates of return periods of 5, 25, 50 and 100 years were considered. No data is available for joint probabilities associating surges and cyclonic wave conditions. Since both increase with stronger cyclonic wind conditions, the return period from the surge used was set at the same return periods used for the wave climate. Although, these events would not typically occur at once, they are strongly correlated. Taking this into account, 12 extreme events have been designed and cover both present and future conditions. The wave and sea level conditions for each extreme event are presented in table 7.

Table 7: Extreme wave condition scenarios

Scenario Event	Abbreviation	Time space	Return period (yrs)	SWH (m)	Period (s)	Tide (m)	Surge (m)	SLR projection	Reef state	SLR added (m)
Extreme Event 1	Ev1ext	Present	5	5.0	10.5	0.4	0.16	N/A	Good	0
Extreme Event 2	Ev2ext	Present	25	6.0	10.8	0.4	0.33	N/A	Good	0
Extreme Event 3	Ev3ext	Present	50	6.4	10.9	0.4	0.43	N/A	Good	0
Extreme Event 4	Ev4ext	Present	100	6.8	11.0	0.4	0.54	N/A	Good	0
Extreme Event 5	Ev5ext	Future	5	5.0	10.5	0.4	0.16	RCP4.5	Poor	0.52
Extreme Event 6	Ev6ext	Future	25	6.0	10.8	0.4	0.33	RCP4.5	Poor	0.52
Extreme Event 7	Ev7ext	Future	50	6.4	10.9	0.4	0.43	RCP4.5	Poor	0.52
Extreme Event 8	Ev8ext	Future	100	6.8	11.0	0.4	0.54	RCP4.5	Poor	0.52
Extreme Event 9	Ev9ext	Future	5	5.0	10.5	0.4	0.16	RCP8.5	Poor	0.68
Extreme Event 10	Ev10ext	Future	25	6.0	10.8	0.4	0.33	RCP8.5	Poor	0.68
Extreme Event 11	Ev11ext	Future	50	6.4	10.9	0.4	0.43	RCP8.5	Poor	0.68
Extreme Event 12	Ev12ext	Future	100	6.8	11.0	0.4	0.54	RCP8.5	Poor	0.68

4.2.3 Choice of location of EraInterim data retrieval

The wave data downloaded from EraInterim for the extreme wave climate was retrieved at coordinates of 57° E and 20.25°S, just off the west coast of Mauritius, for years ranging from 1979-2017. The wave rose at this point is shown in figure 20.

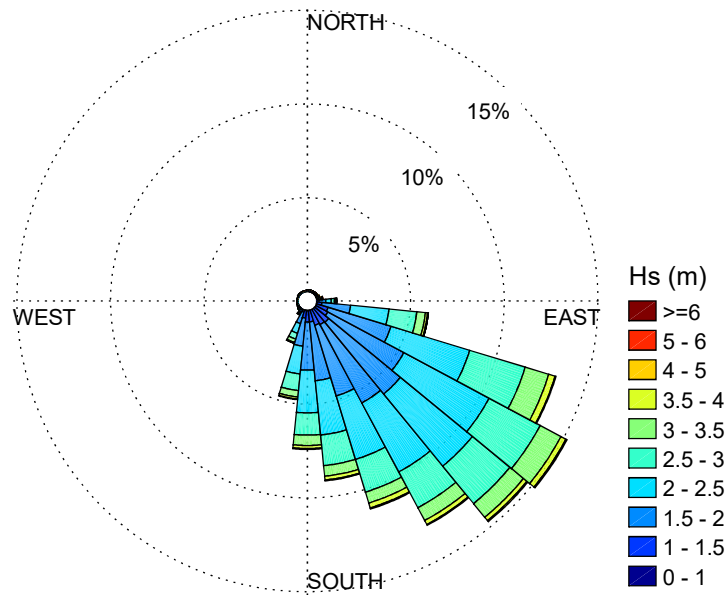


Figure 20: Wave rose from EraInterim data [57° E and 20.25°S] used for the extreme climate

The use of this data is to provide a basis of the existing wave height from storms, in order to draw a projected wave height for a given return period. (See Appendix B.5 for the point of data extraction).

4.2.4 Wave conditions

Two methods to estimate the extreme wave heights for a return period were used: the peak over threshold (POT) and the annual maxima. In both cases, after the determination of the storm wave heights, these were plotted to fit a Weibull distribution curve.

Peak over threshold

The POT method requires that one SWH and corresponding period is extracted from the data time series for each storm. To be considered a storm, the following conditions should be met:

- 1- The wave height is noted to be higher than the threshold for a duration exceeding 24hrs;
- 2- Two storms cannot occur in the span of 72hrs. If the threshold is exceeded twice, only one value should be used;

Initially, the threshold value was set to extract approximately 5% of the highest waves. Given a normal distribution, the 5% limit of the highest wave data should be found at the sum of the mean and two times the standard deviation.

$$Hs_T = \mu + 2 \times \sigma = 3.37 \text{ m}$$

Hs_T = Threshold significant wave height, μ = mean, σ = Standard deviation

The threshold was increased to 4m, to better represent the number of cyclonic wave events expected to affect Mauritius. The Southern Indian Ocean counts approximately 9 cyclones/year, and only a portion affect Mauritius' wave climate. The increased threshold generates an average of 1.9 events/year, which sounds reasonable. Also with a changed threshold, the error between the data and a fitted Weibull curve is reduced.

Annual maxima method

For the annual maxima method, the highest wave height was taken for each year, and in a similar manner, fitted to a Weibull distribution.

Weibull Distribution

The cumulative distribution function of a Weibull distribution is the following:

$$F_x = 1 - e^{-(\frac{x}{\alpha})^\beta}$$

F_x = Cumulative distribution β, α = shape and scale parameters x = random variable

Reducing the equation and taking the natural log on two occasions simplifies the equation to:

$$\ln(-\ln(1 - F_x)) = \beta \ln x - \beta \ln \alpha$$

Which can be expressed as the linear equation, after substitution:

$$y = \beta x' - a$$

To determine the cumulative frequency (F_i) assigned to each storm:

$$F_i = 1 - \frac{i}{n + 1}$$

The fitting of the Weibull distribution curve for the extreme wave height data, allows for values of different return periods to be extrapolated, based on the statistical trend (See Appendix B.6).

Table 8: Significant wave height and mean wave periods for extreme conditions

Method	Return periods (m)							
	5 years		25 years		50 years		100 years	
	swh (m)	mwp (s)	swh (m)	mwp (s)	swh (m)	mwp (s)	swh (m)	mwp (s)
Annual Maxima	5.0	10.3	5.9	10.7	6.2	10.8	6.5	10.9
Peak over Threshold	5.0	10.5	6.0	10.8	6.4	10.9	6.8	11.0

The extreme wave heights using both methods generate similar extreme wave conditions, as presented in table 8. To be conservative, the highest waves and periods from the POT method will be used for the extreme analysis.

Directional coefficients

The mean of the waves within the range of the highest 99 and 99.9 percentile was calculated for each direction. The directional coefficients were then determined by taking the ratio of the directional mean to the highest directional mean. Since the wave count in certain directions is very low, the minimum waves considered was set to 10. In certain cases, this requirement resulted in considering up to 20% of all the waves coming from one direction. Table 9 summarizes the values of the directional coefficients that must be applied to obtain the directional extremes.

Table 9: Directional coefficients

Directions	N	NNE	NE	ENE	E	ESE	SE	SSE	S	SSW	SW	WSW	W	WNW	NW	NNW
Directional coefficients	0.98	0.98	0.90	1.00	0.93	0.83	0.84	0.85	0.85	0.79	0.79	0.72	0.71	0.66	0.85	0.82

The directional coefficients give an indication of the direction in which the highest waves may be expected.

Care in interpretation should nevertheless be taken, since the coefficient does not weigh in the frequency of occurrence. Also, given the limitations of the data (see section 3.4.2.2) certain wave directions are only recorded when high energy waves allow for surpassing the swells and waves occurring simultaneously in other directions. This causes an unweighted ratio of extremes to regular waves between the different directions.

Of all directions, Flic-en-flac is the most exposed to waves approaching perpendicular to the coast, which corresponds to the west direction. Since the accuracy of the directional coefficient is questioned when using EraInterim data, a directional coefficient of 1 will be used, for the westerly approaching wave.

4.2.5 Model domains

For the extreme analysis, the same domains 2 and 3 presented in section 4.1.5 were used, as shown in figure 21.



Figure 21: Domains of the runs for the extreme climate

4.2.6 Tide

When modelling for the extreme climate, the storm tide should be considered. The storm tide is the sum of the storm surge and the predicted tide. In this analysis, to account for the worst case, the highest astronomical tide of 0.4m above LMSL, is used. Since mean tidal levels are high in January to March, which also corresponds to the cyclonic season, using the highest astronomical tide is relevant.

4.2.7 Surge

Two processes contribute to storm surges during extra-tropical cyclones; the strong winds and the low atmospheric pressures. The strong winds blowing over the ocean induce a vertical water circulation phenomenon at the level of the cyclone's eye. When the cyclone reaches shallow waters, the water cannot circulate vertically anymore which results in the increase of the water levels.

The surge conditions for cyclonic events of different return periods were taken from the Baird (2003) report. The determination of these surges was achieved using the records from 25 tropical storms, identifying the pressure deficit for each of them in a first place (Chu & Wang, 1998). Then applying the Empirical Simulation Technique to develop a joint probability between the storms and their response.

Table 10: Surge table (Baird, 2003)

Return Period (yrs)	5	25	50	100
Surge (m)	0.16	0.33	0.43	0.54

5

Numerical model results

5.1 Mean wave climate

The significant wave heights presented for each scenario in this section corresponds to the average of the significant wave heights of 45.4% of all wave conditions. These waves were selected on the basis of directions being susceptible to reach the coast of the study site. If all conditions were considered, the wave height would be significantly lower.

$$H_{smean} = (\sum H_{si} \times f_i) \times \frac{1}{45.4}$$

H_{smean} = Mean significant wave height H_{si} = Significant wave height for each run f_i = freq of occurrence

Table 11: Table of the average SWH inside the lagoon for all scenarios (within approx. 30m from reef and from shore)

	Ref	Sc1	Sc2	Sc3	Sc4	Sc5	Sc6	Sc7
SWH in lagoon (m)	0.031	0.387	0.487	0.653	0.048	0.228	0.307	0.495

The results of the wave evolution over the reef are represented by considering sections over the study area. Please refer to Appendix B.5 to locate section 1 – 3.

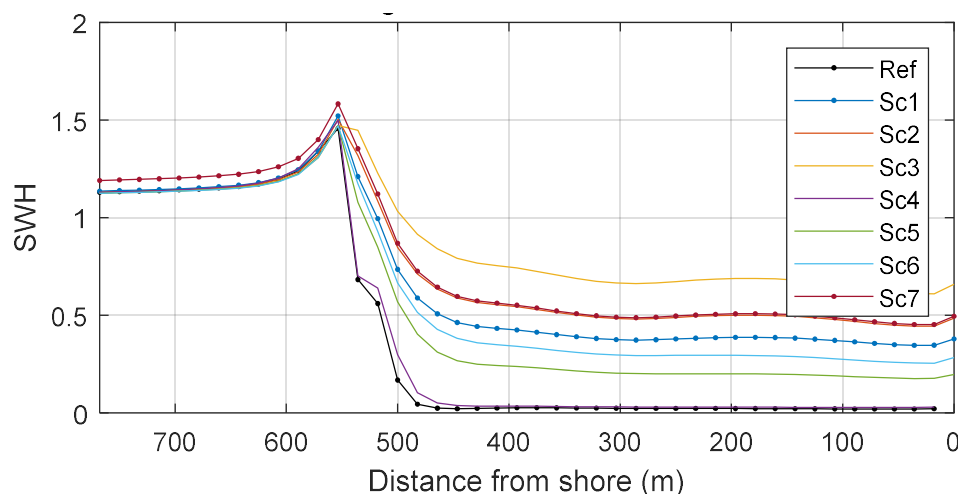
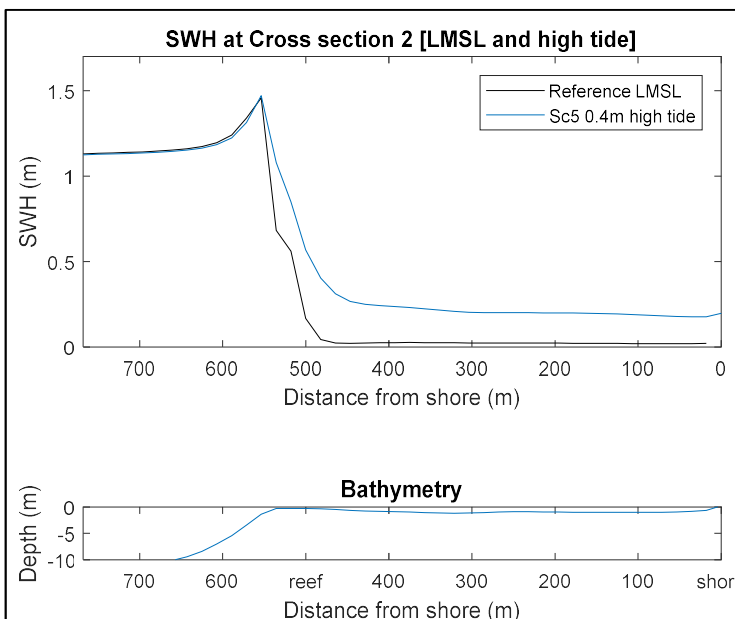


Figure 22: Evolution of the SWH across section 2 for all scenarios

The SWH evolution across the reef is represented at section 2, for all scenarios in figure 22.

5.1.1 Qualitative calibration



The mean SWH inside the lagoon varies between 0.031m and 0.228m for LMSL and high astronomical tides, (table 11). Given a deep water mean wave height of 1.45m the wave heights decay vary between 98% at MSWL and 85% at the highest astronomical tide. Based on Baird (2003) study, a wave height decay of 90% is measured across a reef on the east coast of Mauritius. Péquignet, et al., (2011) measure 97% wave height decay in Guam. Similarly, Ferrario et al., (2014) suggest that 97% wave energy damping by reefs crests on average.

Figure 23: Wave decay at cross section 2 – Upper limit represented with the highest astronomical tide (Sc5)

Figure 23 represents the evolution of the SWH for the current situation at LMSL (Reference scenario) and HAT (Scenario 5).

5.1.2 Tidal effects on energy dissipated

Figure 23 indicates that the processes governing the wave height decay are different LMSL and HAT. During shallower tides, the energy is nearly fully dissipated by the depth induced breaking. From table 12, the energy levels inside the lagoon is 13 times smaller at LSWL, which underlines the high variability of dissipation depending on the tidal variations, even in a micro-tidal environment.

Interpretation of SWH changes on figure 23 suggests that shoaling leads to an increase in wave height as it approaches the reef. The wave height then drops when it reaches shallow enough depths causing depth induced breaking. It then travels across the reef flat, where the main actor in damping energy is bottom friction. Once across the flat, the wave height remains relatively stable, with minimal friction induced dissipation throughout the lagoon. Since this is a 2Dimensional cross sectional representation, the lateral wave influences may cause a SWH increase inside the lagoon, as seen in figures 23, 25.

The colour maps in figure 24 and 25 are representations of SWH inside the lagoon for Reference and Scenarios 1 to 7.

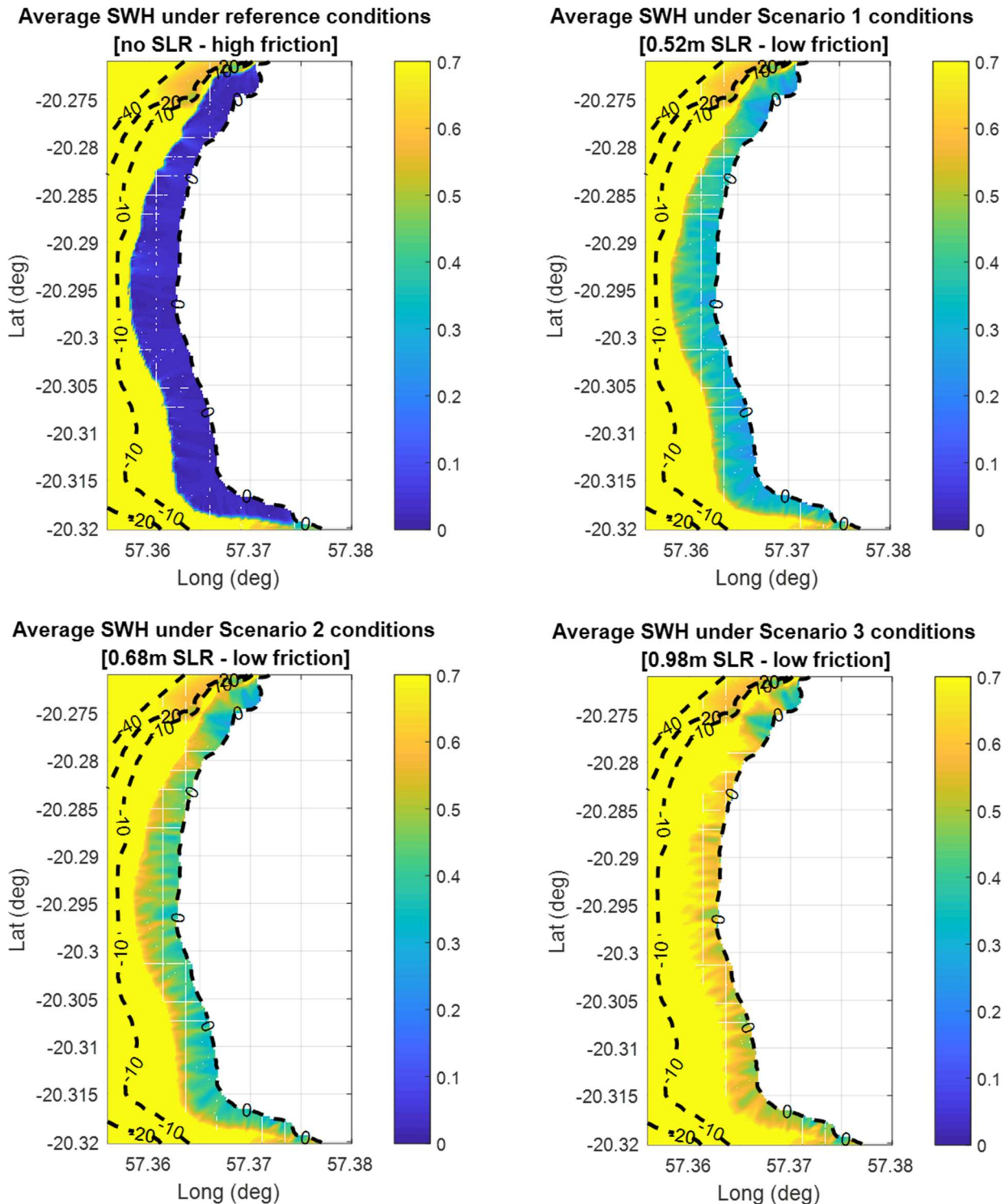


Figure 24: From left to right and top to bottom, Reference, Sc1, Sc2, Sc3 – SWH colour maps

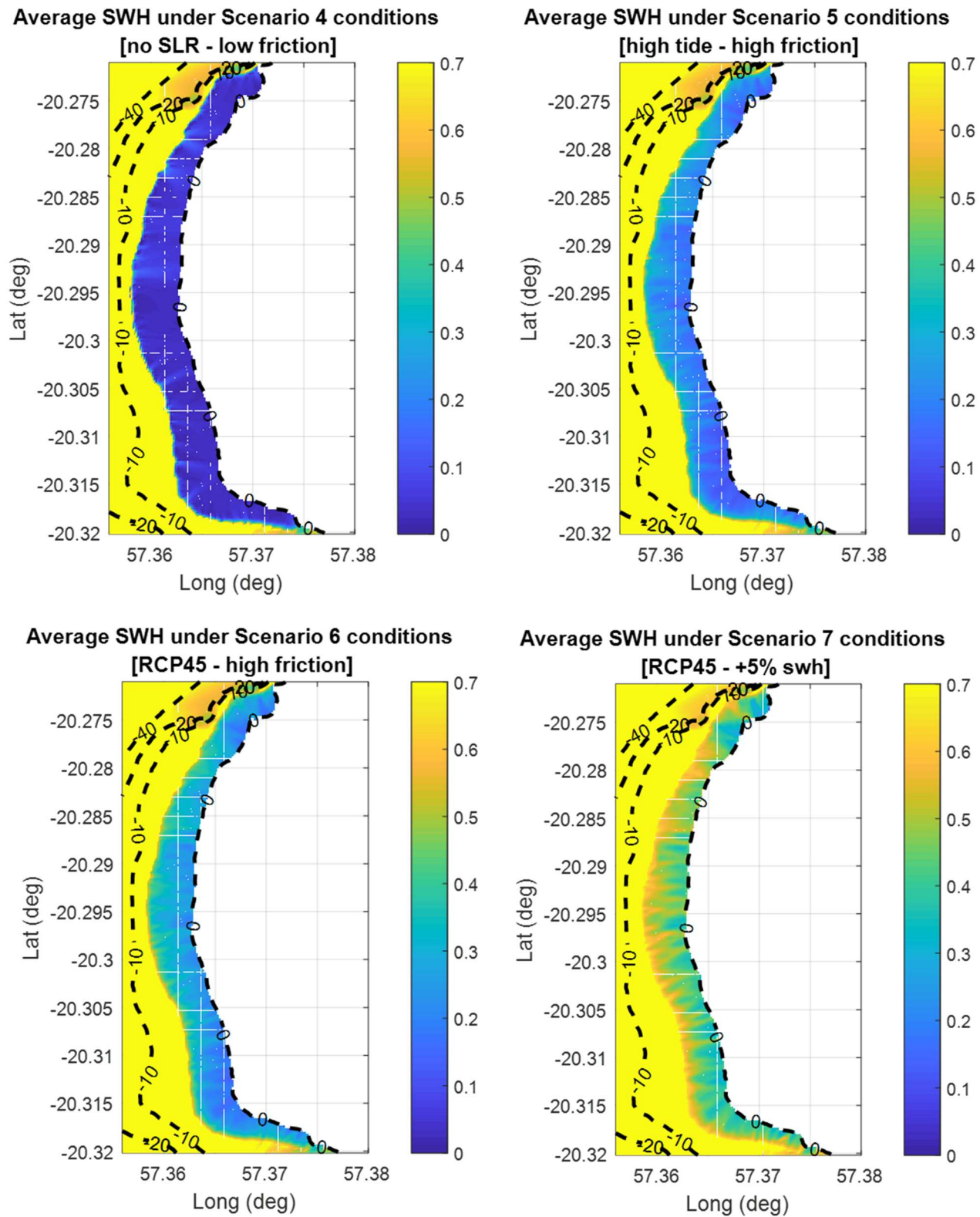


Figure 25: From left to right and top to bottom, Sc4, Sc5, Sc6, Sc7 – SWH colour maps

5.1.3 SLR effects on SWH

The comparison of the reference condition to the three SLR cases, Sc1-3 is shown in the figure 26.

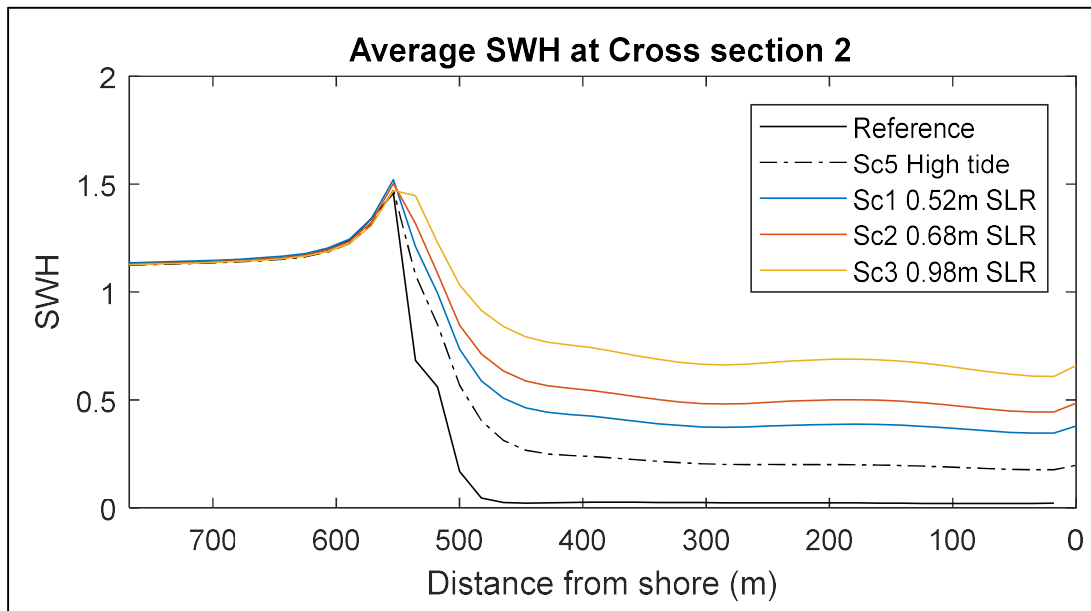


Figure 26: SWH at scenarios 1-3 & 5 along section 2

Under the SLR Scenarios 1 to 3, the wave heights are seen to increase significantly in the lagoon, relative to the Reference and High tide cases. As expected, the higher the SLR, the higher the waves protruding inside the lagoon, as larger wave heights are sustained across the reef. At LSWL, the waves are nearly entirely dissipated, while for the highest sea level increase of 0.98m, there is only 55% of incoming wave height reduction. The increased water levels induce less energy dissipated from depth induced breaking. For a given wave height, at a given location, if the water depth is increased over the reef flat, there will be a reduction in the near bed orbital velocities and in turn the shear stress and bottom friction will decrease.

Note a shift towards the shoreline in the SWH peak for Sc3 relative to the reference case, which indicates that wave breaking would happen closer to the reef flat. Changes in water levels induce changes in the localization of the processes occurring.

Figure 27 shows the location of the points for which SWH were retrieved from to construct the plot in figure 28. Figure 28, is plotted from the SWH observed at points 1.A, 2.A, 3.A. Each line plotted, connects SWH measured for different scenarios of varying SLR, only. The solid lines are for scenarios with friction coefficients for an eroded reef state. The dotted lines are for scenarios with the current reef state. The wave heights were taken from the Reference, Sc1-3 and 5 and 6.

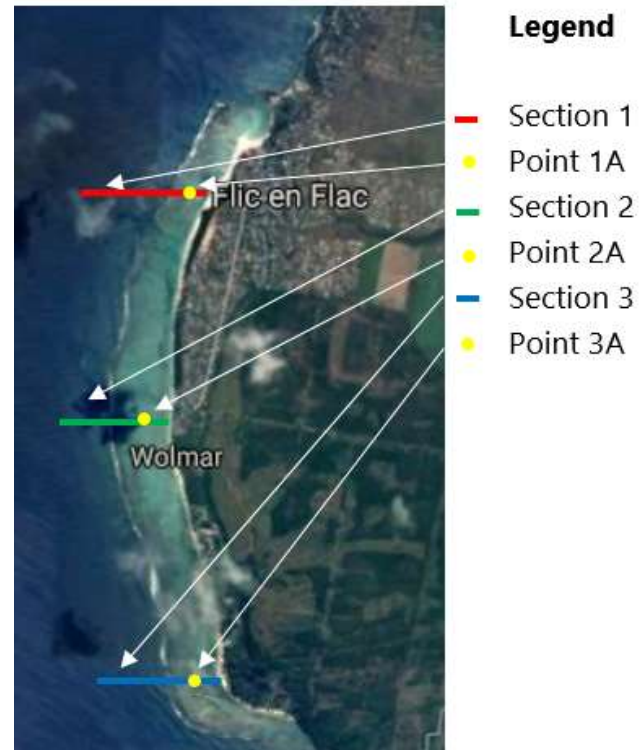
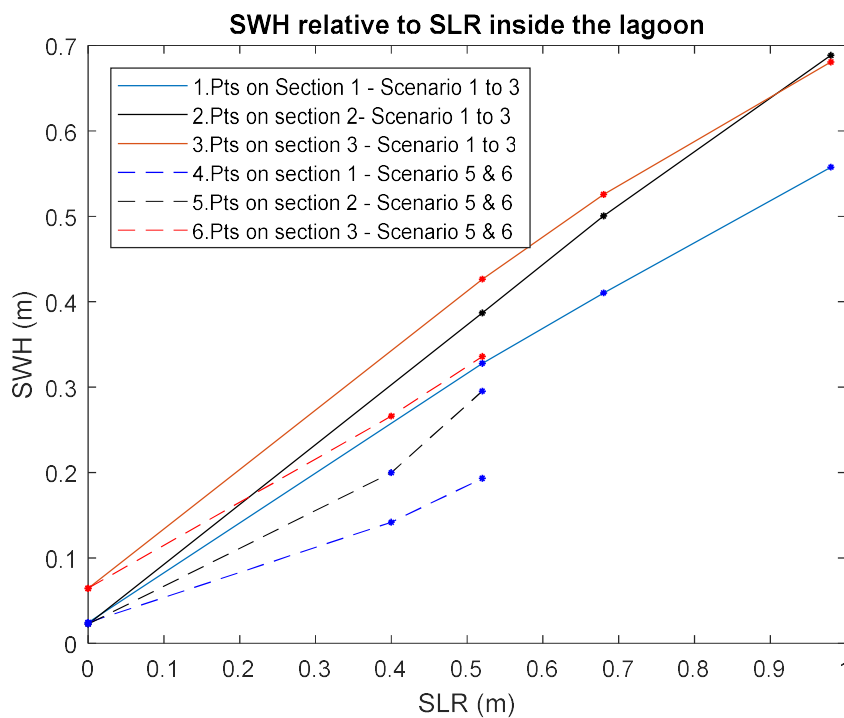


Figure 27: Location of points used in the analysis of figure 28



The trend of the increase in SWH is observed to be more or less linear with the increase of water levels (as seen on lines 1, 2 and 3), at the three sections inside the lagoon.

The proportion of SWH change due to bottom friction can be visualized by the distance between each pair of solid and dotted lines (1. & 4., 2. & 5., 3. & 6.) in figure 28.

Figure 28: SWH vs SLR scenarios – from the SWH at a point given Sc1-3, 5, 6 results

The contribution to wave height decay, of the friction coefficient variations may be estimated by comparing the SWH at points in the lagoon for scenarios 1 and 6. The wave height decay for a higher friction coefficient contributes to 41%, 23% and 19%, for sections 1, 2 and 3, respectively, given 0.52m of SLR conditions.

5.1.4 Friction coefficient

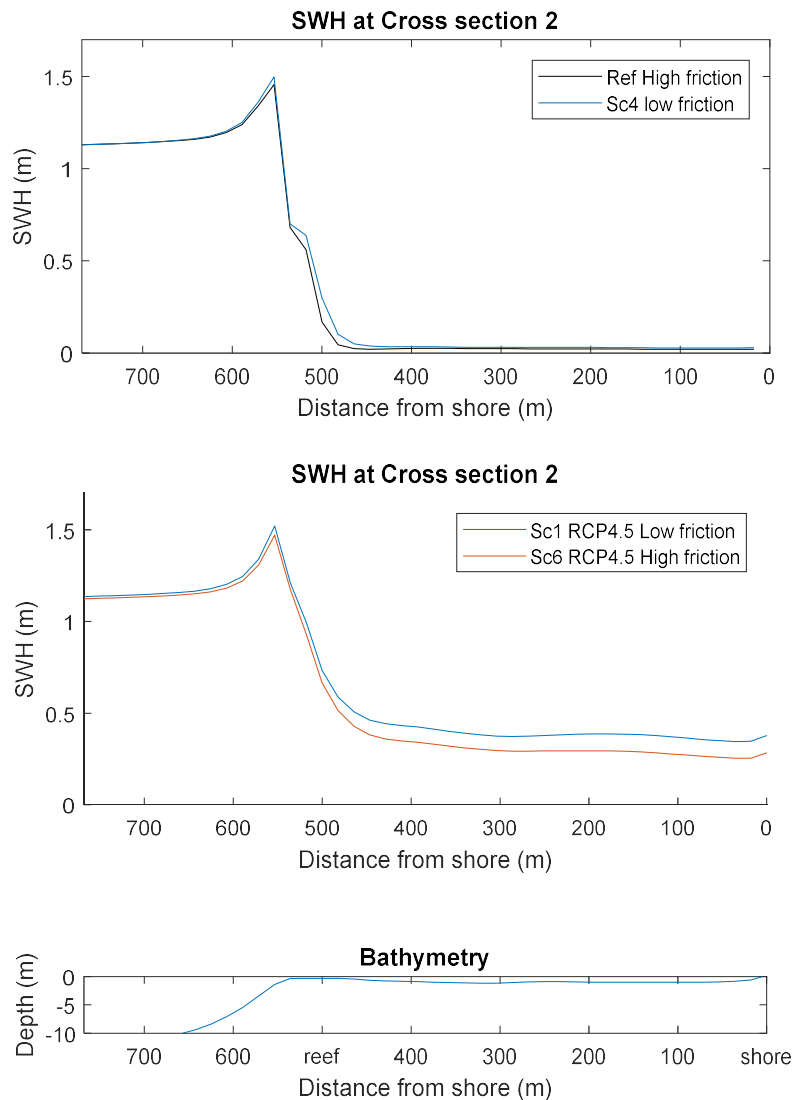


Figure 29: Evolution of SWH across section 2 for scenarios of varying friction coefficient

As surface-gravity waves approach from deep water, bottom friction reduces the SWH gradually across the fore reef. Wave height decay from friction has its highest influence when wave traverses over the reef flat. For a given wave, the shallower the water depth, the larger the portion of the water column the boundary layer will account for, and the higher the orbital velocities interacting with the sea floor. The effect of friction inside the lagoon is much less significant, since the water

Two sets of scenarios have similar input parameters other than their friction coefficient. The reference case and scenario 4 are modelled under LMSL and scenario 1 and 6 under mean RCP4.5 SLR. The difference between the SWH of each scenario provides an indication of the effects of higher bottom friction, represented in figure 29.

In oscillatory flow conditions, the boundary layer is in the order of a few centimeters above the bed. The small layer thickness is a result of the current directions reversing frequently. High vertical velocity gradients exist at the boundary layer interface resulting in large stresses within the layer.

depth increases after traversing the reef flat. The wave decay induced from friction prior to breaking is not a significant contributor to the wave height inside the lagoon, since at breaking the governing parameter defining the wave post breaking is the depth, and not the wave height approaching.

The plot of the cumulative changes in SWH of the difference between two scenarios of different friction factors enables to visualize the effects of a higher frictional coefficient, as shown in figure 30. The higher the positive rate of change of the difference, the higher the frictional wave induced dissipation across the section.

$$SWH_{decay} = SWH_{Sc} - SWH_{Ref}$$

As seen on figure 30, higher friction coefficients (f_w) induce higher SWH decay at the fore reef. After breaking, the difference in cumulative SWH diminishes, since depth induced breaking dissipates more energy for the higher wave heights (ie. the scenario having undergone less frictional loss). When the waves travel in the shallow waters across the reef flat, the wave energy loss due to frictional dissipation increases very steeply. Once in the lagoon, the effects of varying bottom friction do not show significant effects on the wave height decay.

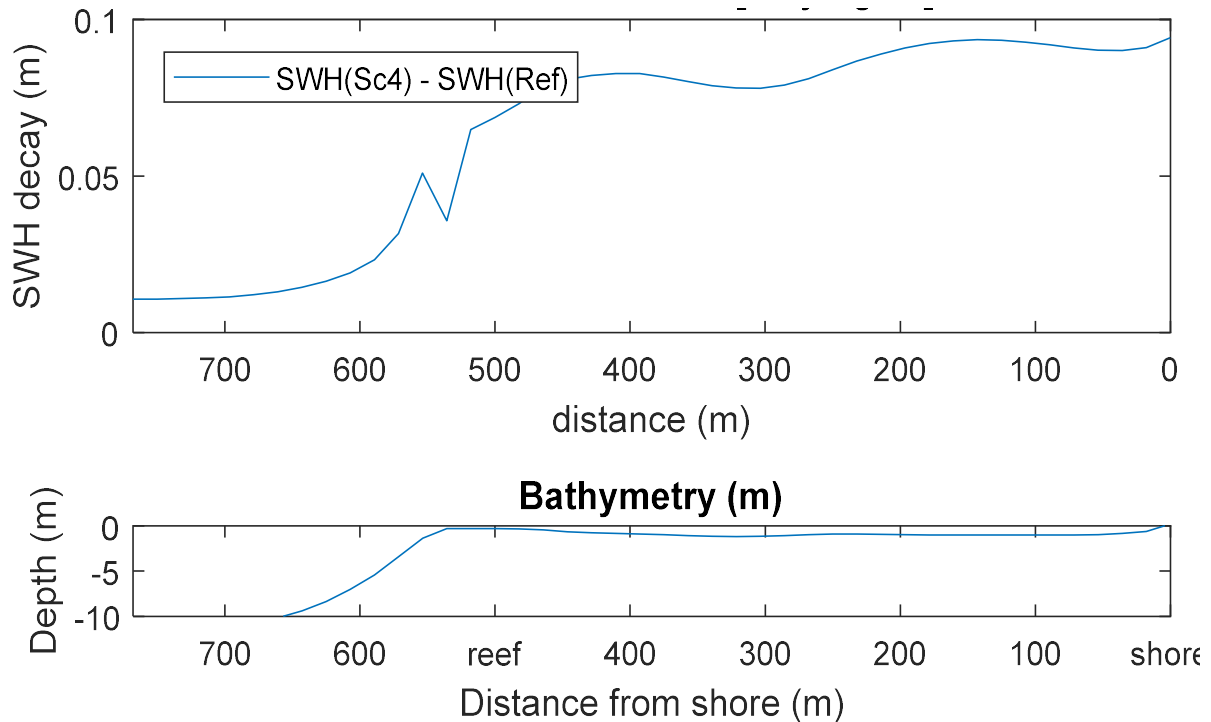


Figure 30: Difference in the SWH between the Reference and Sc4 at section 2 of the reef

5.1.5 Energy levels

The wave energy is related to the square of the SWH. See appendix C1 for the energy representation of all scenarios.

$$E = \frac{\rho g H^2}{8}$$

E = wave energy per square unit area

ρ = water density H = significant wave height

Table 12: Table of the energy per unit surface area inside the lagoon for all scenarios

	Ref	Sc1	Sc2	Sc3	Sc4	Sc5	Sc6	Sc7
Energy per unit area (J/m ²)	1	188	298	536	3	65	118	308

Figure 31 provides a visual representation of the energy differences inside the lagoon for scenarios 1-2 and Reference (note the different scales for each representation).

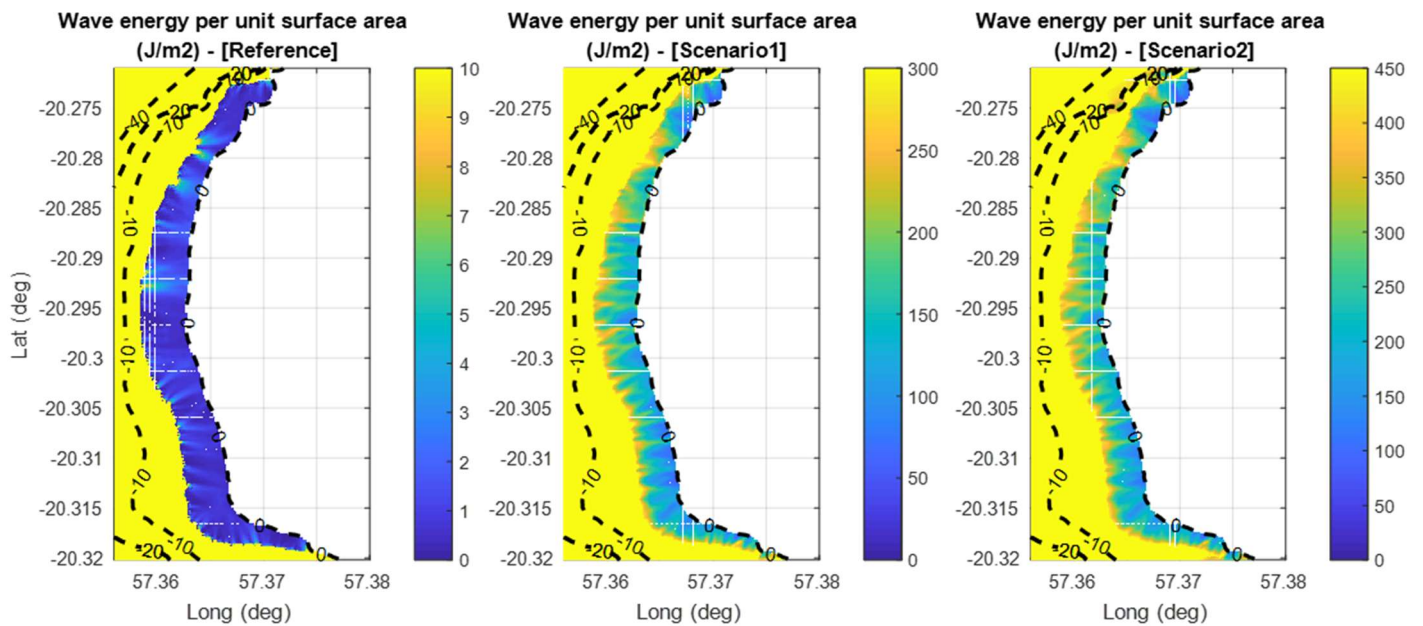


Figure 31: Wave energy per surface area for Ref, Sc1 and Sc2

SWH between Sc1, Sc2 and the HAT scenario are noted to be in the same range. The energy of the HAT is 3 and 9 times smaller than ones calculated for Sc1 and Sc3, respectively. This is due to the quadratic relation of energy to wave heights. Similarly, as a result of the same relation, when comparing wave heights with the Reference results, Sc1 and Sc2 show wave energy approx. 2 orders of magnitude larger.

5.1.6 Effect of wave setup

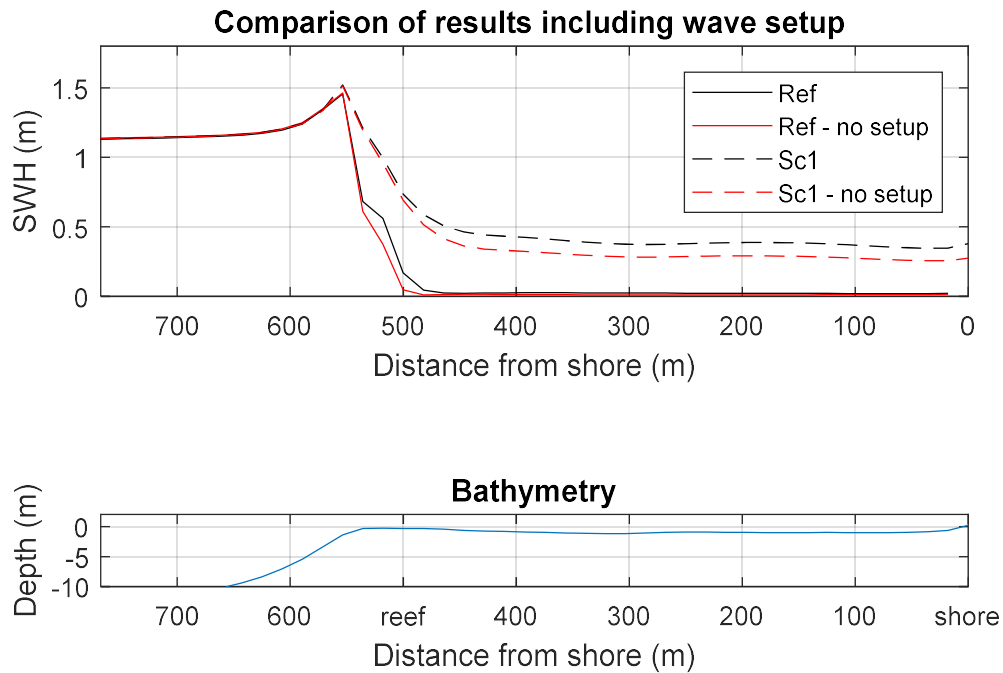


Figure 32: Comparison of setup effects in the reference scenario and scenario 1 at section 2

Wave setup is described as the raising of the mean water level in the surf zone due to a momentum transfer from breaking waves to the water column. In steeply increasing fore reef environments the pressure response in the cross shore momentum balance is higher, as a result of the constrained space in which the wave breaks (Quataert et al., 2015). In figure 32, when comparing Sc1 conditions with and without setup, higher waves are observed inside the lagoon for setup activated SWAN runs. This is expected since wave induced set-up increases the water levels and in turn the depth over the reef flat, reducing depth induced dissipation.

Static wave setup can be expressed as:

$$\frac{\partial \eta}{\partial x} = \frac{1}{\rho g(h + \eta)} \left(-\frac{\partial S_{xx}}{\partial x} + \tau_b \right)$$

η =steady state component of the wave setup

τ_b = bottom friction

The flux of momentum component is expressed by:

$$S_{xx} = \text{Abs} \left(\int_{-h}^{\eta} (p + \rho u^2) dz \right)$$

S_{xx} = radiation stress in the wave propagation direction p = pressure
the integral of ρu^2 accounts for the advection from horizontal particle velocity

Using linear wave theory, the radiation stress in the direction of propagation can be reduced to:

$$S_{xx} = \text{Abs} \left(\int_{-h}^{\eta} (\rho u^2) dz \right) \approx \int_{-h}^{0} (\rho u^2) dz = nE$$

Since setup is directly related to the wave height, and increases with larger incoming waves; setup is of even greater importance during extreme wave events.

5.1.7 Effect of increased wave climate

Scenario 1 and Scenario 7 may be compared to evaluate the effect of a 15% wave height increase at the outer SWAN model boundary. Sc7 shows an increase of 64% and 27% of wave energy and SWH respectively, relative to Sc1. Represented on figure 33.

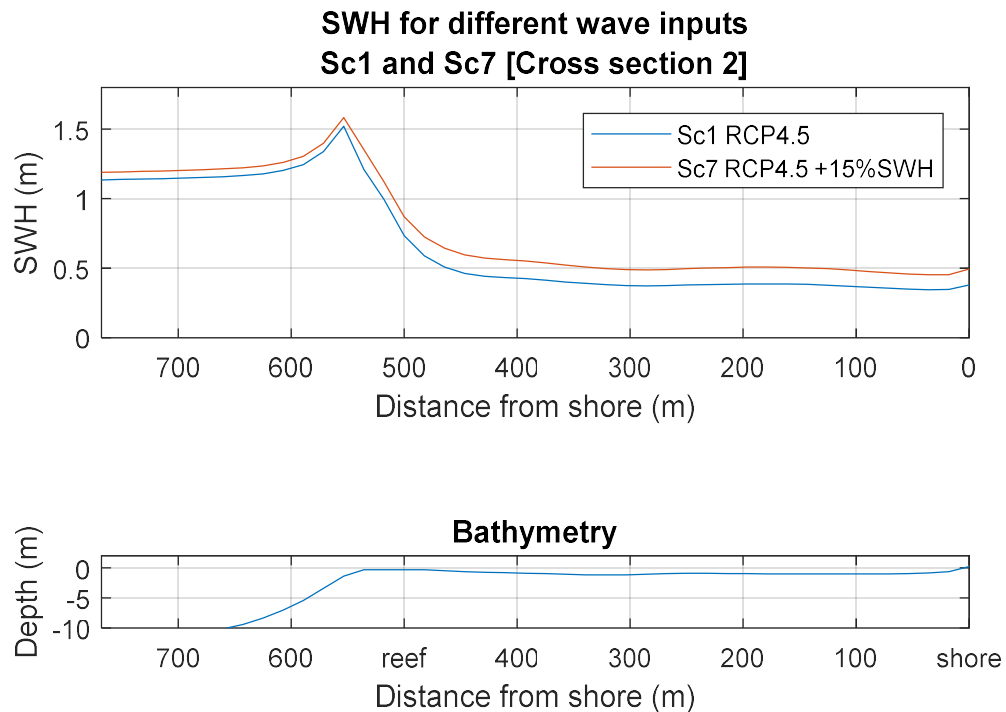


Figure 33: SWH cross section for Sc1 and Sc3 from the fore reef to shore.

Ferrario et al. (2014) suggests that the reef as a whole dissipates energies with linear effect from small to cyclonic waves. Under stationary conditions, Sc1 and Sc7 were found to dissipate 93% and 90% of the incoming wave energy, respectively. To verify that Ferrarios et al. (2014) statement applies for the scenarios considered here, the study would require the consideration of time records where the tidal influence has an effect.

$$E_{decay} = \frac{E_{incidence} - E_{lagoon}}{E_{incidence}}$$

5.2 Extreme wave climate

As anticipated, the larger the cyclonic conditions, the higher the waves inside the lagoon, under all SLR cases. Table 13 presents the SWH inside the lagoon for all events and figure 34 shows evolution of the SWH for events 1 to 4 across the reef.

Table 13: Average SWH and energy per unit area inside the lagoon (within approx. 30m from reef and shore)

Event	Ev1ex	Ev2ex	Ev3ex	Ev4ex	Ev5ex	Ev6ex	Ev7ex	Ev8ex	Ev9ex	Ev10ex	Ev11ex	Ev12ex
SWH (m)	0.57	0.94	0.95	1.07	1.07	1.30	1.42	1.54	1.18	1.41	1.52	1.63
Energy (J/m ²)	408	1111	1134	1439	1439	2124	2534	2981	1750	2499	2904	3339

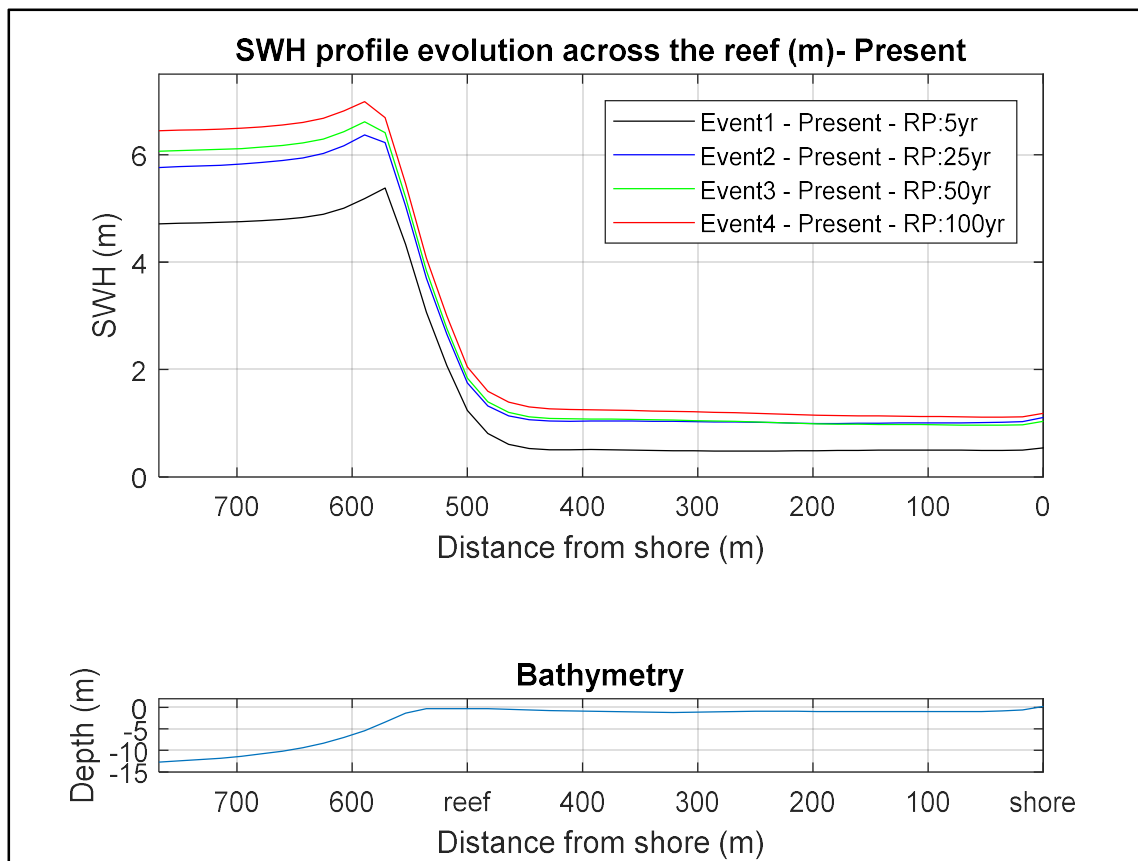


Figure 34: Plot of SWH evolution over reef for wave conditions of different return periods for the present conditions

In this section, results for extreme climatic events under futuristic cases (Event 5-12) are compared to results from the modelled present conditions (Event 1-4) under the same wave conditions. The SWH increase for each extreme wave conditions (RP: 5yrs, 25yrs, 50yrs, 100yrs) is in the range of 38% to 88% and 50% to 107% for SLR defined under RCP4.5 and RCP8.5, respectively. Similarly, the increases of significant wave heights range from 0.36m to 0.50m and 0.47 to 0.61m for SLR defined by the RCP4.5 and RCP8.5, respectively.

Table 14: Percent and absolute increase in mean SWH in the lagoon relative to the extreme scenarios under present conditions

	RCP45 mean SLR		RCP85 mean SLR	
	SWH (relative)	Absolute (m)	SWH	Absolute (m)
Event of RP=5yrs	88%	0.50	107%	0.61
Event of RP=25yrs	38%	0.36	50%	0.47
Event of RP=50yrs	49%	0.47	60%	0.57
Event of RP=100yrs	44%	0.47	52%	0.56

SWH results from the RCP4.5 and RCP8.5 projections are compared to each other for every extreme condition (RP=5, RP=25, RP=50, RP=100). For a 5yr RP an increase of 0.11m is calculated. Similarly for 25yr, 50yr and 100yr RP the increase is comparable, with 0.11m, 0.10m and 0.09m increases, respectively. While knowing that the difference in water levels (from SLR) between both modelled projections is 0.16m. Figures 35 to 36 give a visual SWH representation inside the lagoon for all events and appendix C2 presents the SWH profile evolution across the reef

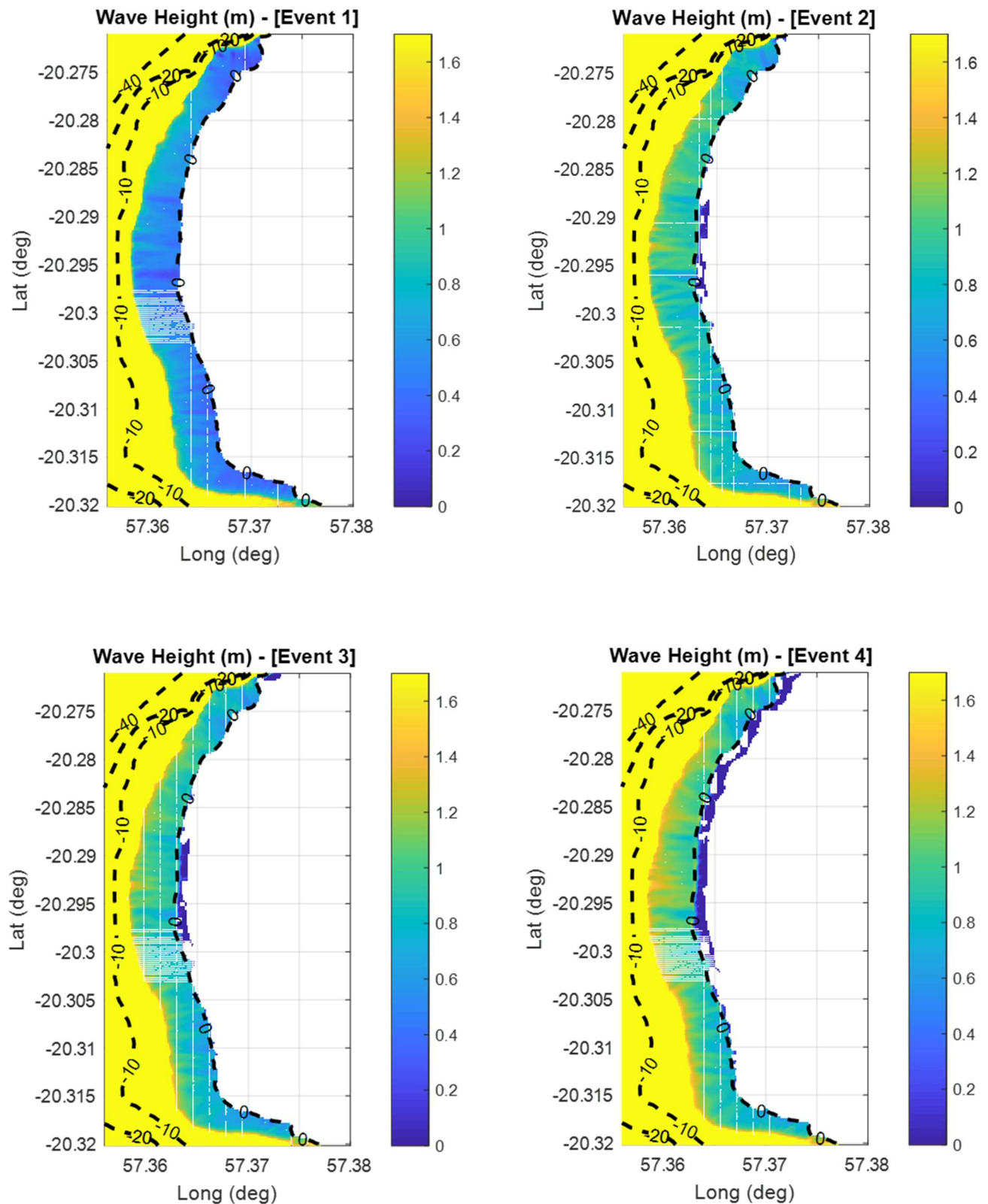


Figure 35: From left to right and top to bottom, Event 1, 2, 3, 4 – SWH color maps

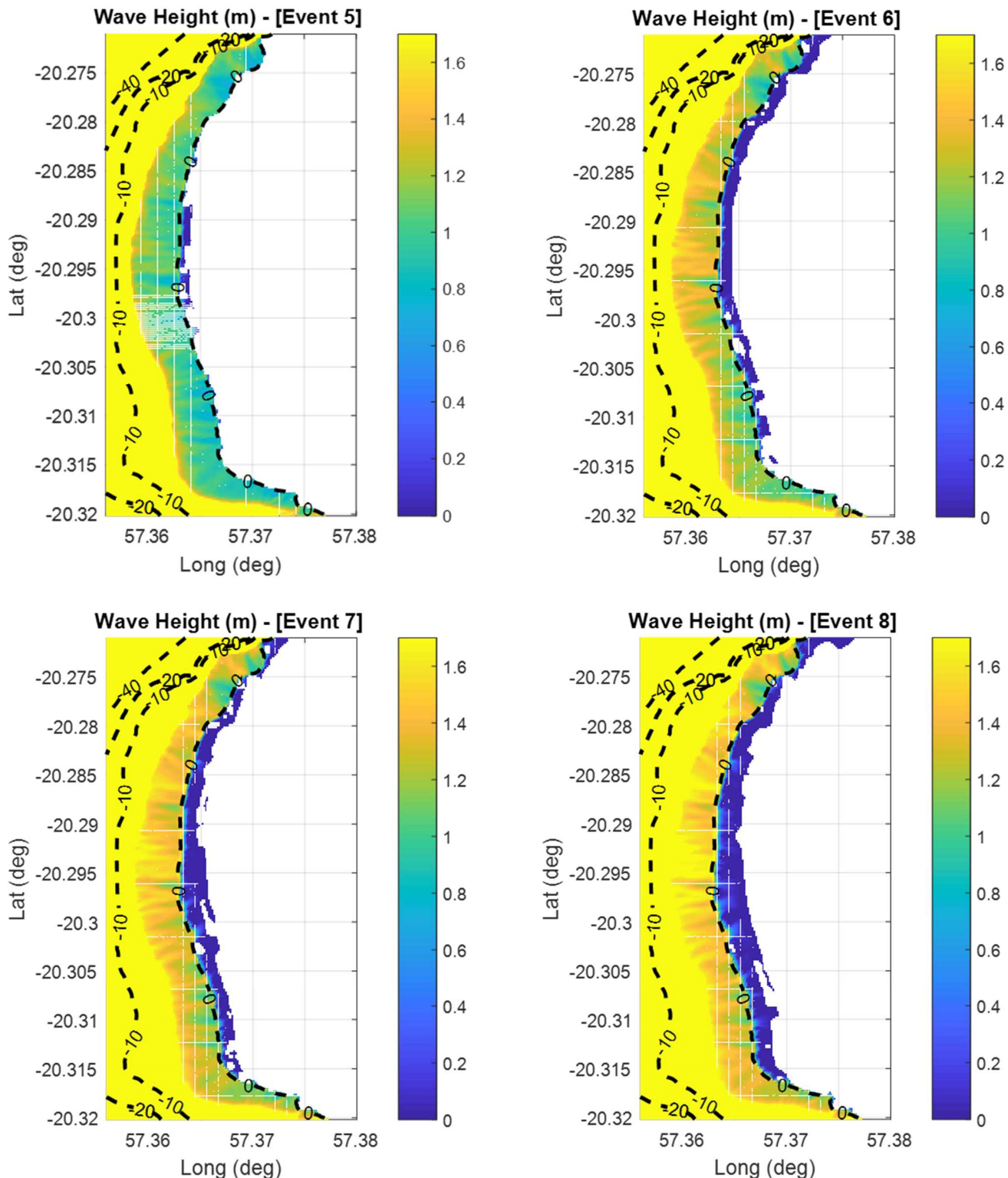


Figure 36: From left to right and top to bottom, Event 5, 6, 7, 8 – SWH color maps

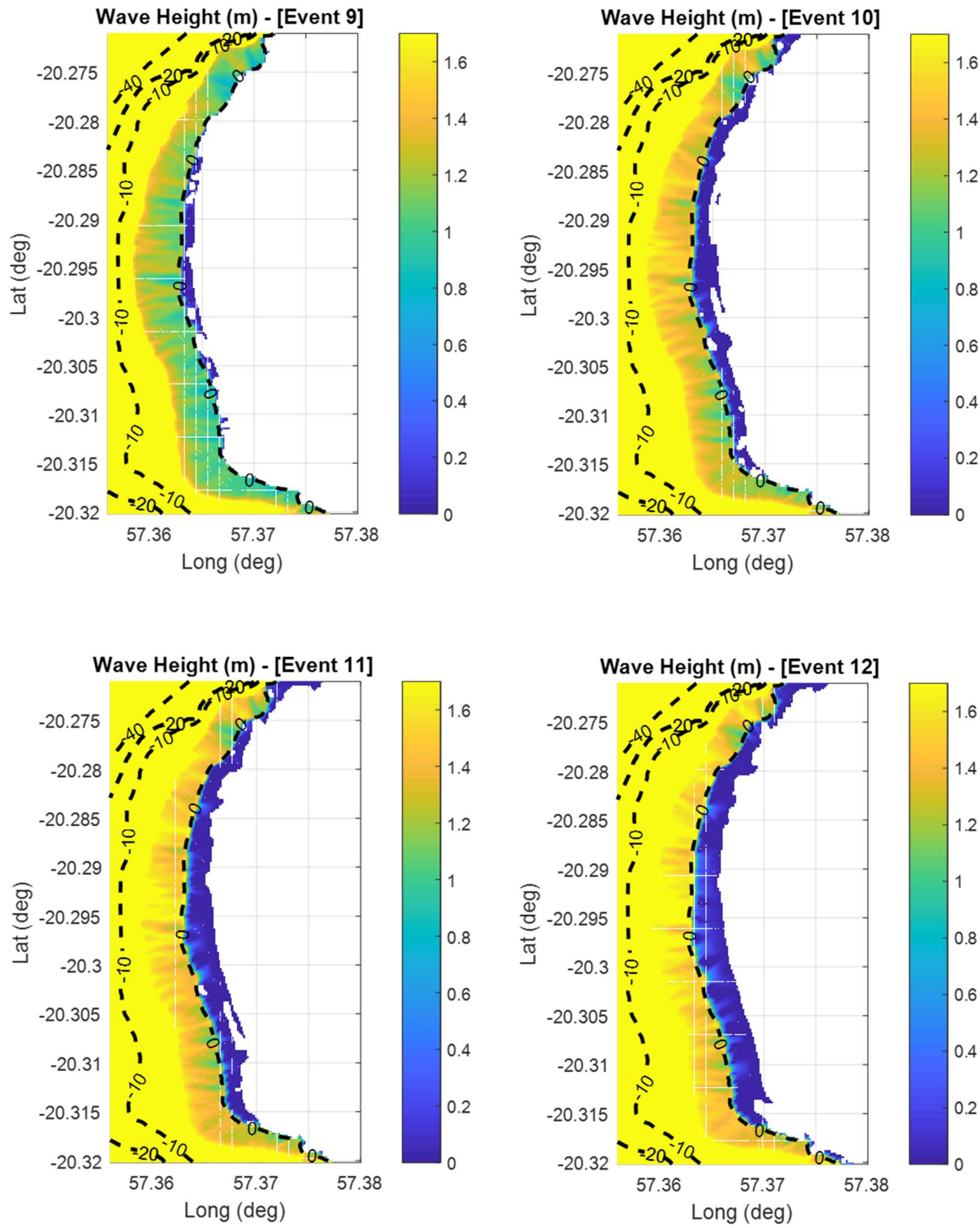


Figure 37: From left to right and top to bottom, Event 9, 10, 11, 12 – SWH color maps

6

Limitations

Limitations encountered were in major part a result of the high level of uncertainty of the wave input wave data used. Unavailability of wave data limits the accuracy in the model outputs.

6.1 Data availability

6.1.1 Wave data

No wave buoy data was available, so global model reanalysis data was used. As mentioned in section 4.1.3, the averaging of wave parameters to a mean significant wave height, mean period and mean direction cause:

- 1- The incapacity of extracting waves approaching in directions shadowed by others of higher energy. This results in a misrepresentation of the waves affecting the study area. Also, limits the accuracy of the calculation for the directional coefficient of the extreme climate.
- 2- The use of global climate reanalysis data at a coordinate south of Mauritius for the mean climate analysis enables to better observe the presence of the waves which will propagate towards the west coast of Mauritius. This allows for a more 'realistic' proportion of waves considered, but as a consequence, the average wave energy input in the model may be overestimated.

The unavailable joint probability of tides and waves resulted in running the model under stationary conditions. Time varying models would have provided tide independent results of the wave height inside the lagoon. In reef like environment, the tide defines the water levels over the reef crest and flat. It therefore dictates which energy dissipation mechanism will occur and to what extent.

Wave conditions calculated from the POT and annual maxima produced wave heights and periods significantly smaller than in other studies. Baird (2003) estimates cyclonic wave heights of 22.2m and periods of 20s using a WAVAD model simulation. Wagner et al. (2003) uses waves of $H_s=13m$ and peak periods of $T_p=14s$ for cyclonic wave conditions of return periods of 100 years, on the west coast of the island (Wagner et al., 2003). Also, the presence of an outlier in the storm data from EraInterim could indicate that considerably larger wave heights do reach Mauritius under cyclonic conditions but are not always represented on the global reanalysis records

6.1.2 Bathymetry

The bathymetry of the reef is extremely complex, and especially in the foreshore, with the presence of spur and grooves. This is where the wave undergoes the largest transformations due to shoaling, refraction, setup and wave breaking. The smoothing of contour lines noticed on the navigational bathymetric charts available suggests that there are large approximations from the interpolation. As a result we expect poor representation of certain features present in the Flic-en-flac, such as the cliffs present on the fore reef.

Constructing a bathymetry surface map is always challenging. The steeply varying bathymetries of the study site, increases the difficulty, requiring an even higher density of independent elevation points to achieve an acceptable level of accuracy.

6.2 Modelling limitations

Built and tested extensively for sandy bottom bathymetries, the use of SWAN does not have the same level of validation for steep and highly complex bathymetries. Although, SWAN is more commonly used outside sub-tropical reef environments, certain studies do indicate the capability of SWAN to accurately model the wave heights and wave setup which occurs when waves propagate over fringing reefs (Filipot & Cheung, 2012). Rogers et al. (2016) also reports high accuracy in modelling the significant wave heights with SWAN in highly frictional and steep environments. Gorrell et al. (2011) uses SWAN in steep underwater canyons and similarly achieves high accuracy in modelling wave heights, directions, periods. In all these cases, calibration was a key to verify the model outputs, but especially important to parameterize the model inputs, such as frictional coefficient and wave breaking coefficients. During shoaling process there is a transfer of energy from the spectral peak to the infragravity band. SWAN is not capable to take into account this spectral alteration.

Under certain conditions, the diffraction parameter resulted in non-convergence of the SWAN model runs. The spatial resolution of the bathymetry should be within a range of 1/5 to 1/10 of the dominant wave length (SWAN, 2017). In the steeply varying bathymetries present at Flic-en-flac, this resolution was not achieved for domain 3 and therefore diffraction was not included for that run.

The bottom friction coefficient used in the study was uniquely based on literature of: 1-coefficients measured over other reefs and 2- reef assessment reports of Flic-en-flac. Given that bottom friction coefficients vary considerably for different environments, a range of error should be accounted for in this analysis, due to this estimation.

6.3 Analysis

As waves of oblique incidence approach the reef from deep water, refraction occurs and the wave crest turn towards the depth contour, gradually reducing the angle of wave incidence. In this study, the wave height decays were mostly analyzed along a straight cross section extending from the lagoon and into intermediate water (cross sections 1-3). Since wave fronts change as they approach the reef, curvilinear sections would better describe the wave evolution. Analyzing wave changes over a straight cross section requires the assumption that the wave fronts are relatively homogeneous in the fore reef. Since the bathymetry dips down in a relatively similar steep manner, at section 2, the error due to misrepresentation is considered small and limited to the fore-reef, where little numerical analysis was carried out.

7

Discussion and conclusion

The SWAN model results indicate a SWH decay within the range of what is found in literature for the Reference and high tide scenario at the Flic-en-flac reef, as measured by Baird (2003) in the reef of Belle Mare. For sea level changes, as per the RCP4.5 and RCP8.5 projections, the model results held up the assumption of that higher wave heights and higher energy levels are transmitted inside the lagoon when water level conditions increase. This is the case for mean wave climates and extreme events.

Depth induced breaking is responsible for most of the energy decay in the modelled conditions representing the present, under both the highest astronomical tide and the LSWL. In higher water levels cases, depth induced breaking dissipates less energy, often resulting in a shift of increasing proportions of energy decay to friction induced, up to a point where friction induced decay would eventually become dominant. Results show that energy dissipation from bottom friction on the fore reef does not contribute significantly to the wave height on the reef flat, since water depths controls the reef flat wave heights. The reef flat and crest are the locations where the highest component of wave friction dissipation occurs, as a result of shallow depths.

Results for scenarios 1-3, show a linear increasing trend in the relation between significant wave heights inside the lagoon and water levels. On the other hand, since energy levels are related to the square of the wave heights; the quadratic relation induces a significantly steeper increase in energy with rising sea levels. For the Sc1 and Sc2 models, the outputs for conditions in 2100 generate an energy increase of 2 orders of magnitude relative to the Reference scenario. When comparing with the results from the highest astronomical tide condition, energy levels are found to be 3 to 9 times higher. This emphasizes the magnitude of changes which could occur. It also, raises the importance of considering the tidal fluctuations in the analysis and how care should be taken when interpreting results from stationary conditions.

The change in wave height input (+5%) was observed to induce a wave height increase of 27% inside the lagoon, when modelled for the scenarios 1 and 7. These results suggest that if the projected increase in the southern storm continues (Gupta et al., 2015) to intensify, the local wave

condition in Flic-en-flac may be significantly affected. Increased wave climate is nevertheless still under considerable uncertainty since the IPCC associates this prediction with a medium level of confidence. Ferrario et al. (2014) states that the whole reef dissipates energy linearly for small to cyclonic waves. If so, the increases in energy levels inside the lagoon can be determined for increasing wave climates, given access to models calibrated over time, from in situ wave data.

The effect of the setup was noted to be of significance in the mean wave climate and extreme wave climate analysis. For the reference scenario including the setup parameter doubled the SWH inside the lagoon, and for Sc1 it increased it by 30%. Based on the model results, the observed effect of the setup on the resultant SWH in the lagoon was of variable increases. Given it induced water levels to rise, this observation was predictable. Baird (2003) identifies wave setup as the biggest water level change driver and estimates it to be within the range of 15% of the deep water wave height, in extreme event conditions.

From an energy dissipation point of view, the higher the bottom roughness and the coral cover complexity present on the flat, the better. This is nevertheless a location which typically cannot sustain a complex 3D bathymetry due to the turbulence of the environment. As building with nature is becoming more relevant nowadays, coral restoration may be an alternative to ensure the coral reefs continue dissipating the incoming waves in Flic-en-flac. Ferrario et al., (2014) finds that restoring reefs is lower in cost than building a low crested breakwater which would provide equivalent coastal protection, on average. Being aware of the energy dissipation processes across the reef will help dictate where to focus the restoration works.

As mentioned, depth induced breaking is responsible for most of the energy dissipation under present conditions. In the scenarios predicting future conditions, the increased water depth over the reef was by consequence the biggest factor in causing an increase in the wave height inside the lagoon. When considering no vertical coral growth, results also suggest that the SWH would on a long term increase more or less linearly with the SLR. This can provide a basis for planning the future. On the other hand, the amount of energy decay due to bottom friction could be compromised much more rapidly and more unpredictably in the event of loss of coral complexity. With predicted increased frequency and intensity of bleaching events (Wang et al., 2014), large scale coral mortality could occur. In the Seychelles, an important amount of coastal erosion has been attributed to loss of the coral complexity, within less than a decade after the 1998 coral bleaching event. The bleaching event caused coral decay and coral rounding, and since considerably more energy was estimated to reach the shores (Sheppard et al., 2005).

Findings in the scenarios which model under water levels at 0.52m above present (RCP4.5) suggest that a bottom roughness decrease from the current reef condition to a degraded one would induce a SWH increase inside the lagoon in the range of 19 to 41%.

Wave breaking generated turbulence intensity varies across the reef with time, when subjected to changing tides and wave conditions. Increase in water levels, will nevertheless cause a permanent shift in the average location of wave breaking closer to the reef flat. This may alter the hydrodynamics of the area and affect the ecosystem.

The results from the cyclonic wave conditions showed larger waves inside the lagoon when the sea level is increased. Under RCP4.5 conditions, the increases relative to present were noted to be around 40 to 50%, and between 50 and 60% when considering RCP8.5 SLR, for return periods of 25, 50, 100yrs. Cyclonic events have had disastrous coastal repercussions, notably after cyclone Carol in 1960. The Flic-en-flac embankment underwent 5 m of cross shore erosion (McIntire & Walker, 1964). Many factors contribute to coastal damage of a cyclone including: the surge, heavy rainfall, strong winds, wave setup. Nonetheless, under deteriorating reefs and sustained sea level rise, the wave conditions should be expected to increase and have higher repercussions for any given cyclonic event.

The overall results of this report suggest that more energy would traverse over the reef under the IPCC projected conditions in 2100, in Flic-en-flac. The consequences of hydrodynamics changes may affect coastal defense, fisheries, recreation by causing habitat and diversity losses, change in the shoreline, erosion, and increased hazard risks (Ferrario et al., 2014). With time varying calibrated models from field data, the effects of SLR and coral reef deterioration on the hydrodynamics in the lagoon would help for best planning and management for the near and long term future conditions.

8

References

- Baird, W. F. (2003). Study on Coastal Erosion in Mauritius, 1(August).
- Chu, P.-S., & Wang, J. (1998). Modeling Return Periods of Tropical Cyclone Intensities in the Vicinity of Hawaii*. *Journal of Applied Meteorology*, 37(9), 951–960. [https://doi.org/10.1175/1520-0450\(1998\)037<0951:MRPOTC>2.0.CO;2](https://doi.org/10.1175/1520-0450(1998)037<0951:MRPOTC>2.0.CO;2)
- Church, J. a., Clark, P. U., Cazenave, a., Gregory, J. M., Jevrejeva, S., Levermann, a., ... Unnikrishnan, a. S. (2013). Sea level change. *Climate Change 2013: The Physical Science Basis. Contribution of Working Group I to the Fifth Assessment Report of the Intergovernmental Panel on Climate Change*, 1137–1216. <https://doi.org/10.1017/CBO9781107415315.026>
- Daby, D. (2003). Effects of seagrass bed removal for tourism purposes in a Mauritian bay. *Environmental Pollution*, 125(3), 313–324. [https://doi.org/10.1016/S0269-7491\(03\)00125-8](https://doi.org/10.1016/S0269-7491(03)00125-8)
- Dhunny, A. Z., Lollchund, M. R., & Rughooputh, S. D. D. V. (2015). Long-Term Wind Characteristics at Selected Locations in Mauritius for Power Generation. *Journal of Wind Energy*, 2015(November 2016), 1–12. <https://doi.org/10.1155/2015/613936>
- Ferrario, F., Beck, M. W., Storlazzi, C. D., Micheli, F., Shepard, C. C., & Airoldi, L. (2014). The effectiveness of coral reefs for coastal hazard risk reduction and adaptation. *Nature Communications*, 5(May), 1–9. <https://doi.org/10.1038/ncomms4794>
- Filipot, J. F., & Cheung, K. F. (2012). Spectral wave modeling in fringing reef environments. *Coastal Engineering*, 67, 67–79. <https://doi.org/10.1016/j.coastaleng.2012.04.005>
- Fleming, K., Johnston, P., Zwart, D., Yokoyama, Y., Lambeck, K., & Chappell, J. (1998). Refining the eustatic sea-level curve since the Last Glacial Maximum using far- and intermediate-field sites. *Earth and Planetary Science Letters*. [https://doi.org/10.1016/S0012-821X\(98\)00198-8](https://doi.org/10.1016/S0012-821X(98)00198-8)
- Gehrels, Roland, W., & Woodworth, P. L. (2013). When did modern rates of sea level start? *Elsevier, Global and*(Volume 100), Pages 263-277.
- Gorrell, L., Raubenheimer, B., Elgar, S., & Guza, R. T. (2011). SWAN predictions of waves observed in shallow water onshore of complex bathymetry. *Coastal Engineering*, 58(6), 510–516. <https://doi.org/10.1016/j.coastaleng.2011.01.013>
- Gupta, N., Bhaskaran, P. K., & Dash, M. K. (2015). Recent trends in wind-wave climate for the Indian Ocean. *Current Science*, 108(12), 2191–2201.
- Holthuijen, L. H. (2010). *Waves in oceanic and coastal waters*.
- Ineda, J. A. B. E., Uis, J. O. S. E. L., & Tefanoni, H. E. (2007). Comparing the performance of two spatial interpolation methods for creating a digital bathymetric model of the Yucatan submerged platform. *Journal of Aquatic Sciences*, 2(3), 247–254. Retrieved from [http://www.panamjas.org/pdf_artigos/PANAMJAS_2\(3\)_247-254.pdf](http://www.panamjas.org/pdf_artigos/PANAMJAS_2(3)_247-254.pdf)

- IPCC. (2014). *Summary for Policymakers. Climate Change 2014: Synthesis Report. Contribution of Working Groups I, II and III to the Fifth Assessment Report of the Intergovernmental Panel on Climate Change.* <https://doi.org/10.1017/CBO9781107415324>
- JICA. (2015). *the Project for Capacity Development on Coastal Protection and Rehabilitation in the Republic of Mauritius Final Report the Project for Capacity Development on Coastal Protection and Rehabilitation in the Republic of Mauritius.*
- Kristensen, T. B., Huuse, M., Piotrowski, J. a, & Clausen, O. R. (2007). A morphometric analysis of tunnel valleys in the eastern North Sea based on 3D seismic data. *Journal of Quaternary Science*, 22(8), 801–815. <https://doi.org/10.1002/jqs>
- Lowry, R., Pugh, D. T., & Wijeratne, E. M. S. (2008). Observations of Seiching and Tides Around the Islands of Mauritius and Rodrigues. *Western Indian Ocean Journal of Marine Science*.
- Mauritius Meterological Services. (2018). Tidal Predictions in Mauritius for May and June 2018. Retrieved May 15, 2018, from <http://metservice.intnet.mu/sun-moon-and-tides-tides-mauritius.php>
- McIntire, W. G., & Walker, H. J. (1964). Tropical cyclones and coastal morphology in Mauritius. *Annals of the Association of American Geographers*, 54(4), 582–596.
- MMCS. (2010). *Etude de faisabilité pour la mise en place d'une ou plusieurs aires marine protégées sur la côte sud-ouest de Maurice(cartographie des habitats et de la valeur patrimoniale).*
- Monismith, S. G., Rogers, J. S., Kowek, D., & Dunbar, R. B. (2015). Frictional wave dissipation on a remarkably rough reef. *Geophysical Research Letters*, 42(10), 4063–4071. <https://doi.org/10.1002/2015GL063804>
- Naseef, T. M., & Kumar, V. S. (2017). Variations in return value estimate of ocean surface waves - A study based on measured buoy data and ERA-Interim reanalysis data. *Natural Hazards and Earth System Sciences*, 17(10), 1763–1778. <https://doi.org/10.5194/nhess-17-1763-2017>
- NCAR. (2011). Introduction to tropical meterology. Retrieved June 8, 2018, from http://www.chanthaburi.buu.ac.th/~wirote/met/tropical/textbook_2nd_edition/navmenu.php_tab_4_page_2.3.0.htm
- NOAA. (2017). coral reef cross section. Retrieved from https://oceanservice.noaa.gov/education/kits/corals/media/supp_coral04b.html
- Osorio-Cano, J. D., Osorio, A. F., & Peláez-Zapata, D. S. (2017). Ecosystem management tools to study natural habitats as wave damping structures and coastal protection mechanisms. *Ecological Engineering*. <https://doi.org/10.1016/j.ecoleng.2017.07.015>
- Péquignet, A. C., Becker, J. M., Merrifield, M. A., & Boc, S. J. (2011). The dissipation of wind wave energy across a fringing reef at Ipan, Guam. *Coral Reefs*, 30(SUPPL. 1), 71–82. <https://doi.org/10.1007/s00338-011-0719-5>
- Quataert, E., Storlazzi, C., Van Rooijen, A., Cheriton, O., & Van Dongeren, A. (2015). The influence of coral reefs and climate change on wave-driven flooding of tropical coastlines. *Geophysical Research Letters*, 42(15), 6407–6415. <https://doi.org/10.1002/2015GL064861>
- Ragoonaden, S. (1997). Impact of sea-level rise on Mauritius. *Journal of Coastal Research*, (24), 205–223.
- Romagnoli, P., Pisani, P., Pasqua, C., & Mazzoleni, G. (2015). *Opportunity Assessment for the development of Geothermal Energy in Mauritius* (Vol. 2009).
- Sheppard, C., Dixon, D. J., & Sheppard, R. P. (2005). Coral mortality increases wave energy reaching shores protected by reef flats: Examples from the Seychelles. *Elsevier*.
- Shigeru, A., Kostianoy, A., & Talley, L. (2013). *Climate change 2103: the Physical science basis. Chapter 3 - Observations: Ocean. Climate Change 2013 - The Physical Science Basis.* <https://doi.org/10.1017/CBO9781107415324.010>

- Simon J. Holgate, Andrew Matthews, Philip L. Woodworth, Lesley J. Rickards, Mark E. Tamisiea, Elizabeth Bradshaw, Peter R. Foden, Kathleen M. Gordon, Svetlana Jevrejeva, and J. P. (2013). New data systems and products at the permanent service for mean sea level. *Journal of Coastal Research*, 29(3), 493–504. <https://doi.org/doi:10.2112/JCOASTRES-D-12-00175.1>
- SWAN. (2017). SWAN: Scientific and technical Documentation. Retrieved from <http://swanmodel.sourceforge.net/download/zip/swantech.pdf>
- Swan, T. (2009). USER MANUAL SWAN - Cycle III version 41.01A. *Cycle*, 126.
- van Dongeren, A., Lowe, R. J., Pomeroy, A., Trang, D. M., Roelvink, D., Symonds, G., & Ranasinghe, R. (2013). Numerical modeling of low-frequency wave dynamics over a fringing coral reef. *Coastal Engineering*, 73, 178–190.
- Wagner, C., Bay, N., Rouge, M., & Louis, P. (2003). INVESTIGATIONS OF CYCLONE WAVE CLIMATE AND OVERTOPPING AT THE CONTAINER TERMINAL, PORT LOUIS, MAURITIUS Doug Treloar 1 , Michael Coull 2 , David Taylor 1 and S. Goburdhone 3, (154), 1–10.
- Wang, X., Broch, O. J., Forbord, S., Handå, A., Skjermo, J., Reitan, K. I., ... Olsen, Y. (2014). Assimilation of inorganic nutrients from salmon (*Salmo salar*) farming by the macroalgae (*Saccharina latissima*) in an exposed coastal environment: Implications for integrated multi-trophic aquaculture. *Journal of Applied Phycology*, 26(4), 1869–1878. <https://doi.org/10.1007/s10811-013-0230-1>
- Wong, P. P., Losada, I. J., Gattuso, J.-P., Hinkel, J., Khattabi, A., McInnes, K. L., ... Sallenger, A. (2014). *Coastal systems and low-lying areas. In: Climate Change 2014: Impacts, Adaptation, and Vulnerability. Part A: Global and Sectoral Aspects. Contribution of Working Group II to the Fifth Assessment Report of the Intergovernmental Panel on Climate Change.*
- Xin, L. H., Adzis, K. A. A., Hyde, J., & Cob, 1Zaidi C. (2016). *Growth performance of Acropora formosa in natural reefs and coral nurseries for reef restoration. AACL Bioflux*. Retrieved from <http://www.bioflux.com.ro/docs/2016.1090-1100.pdf>